Slowing Rates of Regional Exhumation in the Western Himalaya: Fission Track Evidence from the Indus Fan

Peng Zhou[1], Andrew Carter[2], Yuting Li[1], Peter D. Clift[1,3]

1- Department of Geology and Geophysics, Louisiana State University, Baton Rouge 70803, USA
2- Department of Earth and Planetary Sciences, Birkbeck College, University of London, London WC1E 7HX, UK
3- Research Center for Earth System Science, Yunnan University, Kunming, Yunnan Province, 650091, China

Abstract

We use apatite fission track (AFT) ages from sediments recovered by International Ocean Discovery Program in the Laxmi Basin, Arabian Sea, to constrain exhumation rates in the western Himalaya and Karakoram since 15.5 Ma. With the exception of a Triassic population in the youngest 0.93 Ma samples AFT ages are overwhelmingly Cenozoic, largely <25 Ma, consistent with both a Himalaya-Karakoram source and rapid erosion. Comparison of the minimum cooling age of each sample with depositional age (lag time) indicates an acceleration in exhumation between 7.8 and 7.0 Ma, with lag times shortening from ~6.0 m.y. between 8.5 and 7.8 Ma to being within error of zero between 7.0 and 5.7 Ma. Sediment supply at that time

was largely from the Karakoram and to a lesser extent the Himalaya based on U-Pb zircon ages from the same samples. This time coincides with a period of drying in the Himalayan foreland caused by weaker summer monsoons and Westerly winds. It also correlates with a shift of erosion away from the Karakoram, Kohistan and the Tethyan Himalaya towards more erosion of the Lesser, Greater Himalaya and Nanga Parbat, as shown by zircon U-Pb provenance data and especially after 5.7 Ma based on Nd isotope data. Samples younger than 7.0 Ma have lag times ~4.5 m.y., similar to Holocene Indus delta sediments.

Keywords: International Ocean Discovery Program, Fission track, erosion, Himalaya, Indus Fan, monsoon

Introduction

If we are to understand how the evolving climate of Asia has impacted the tectonic development of the Himalaya and Tibetan Plateau, or vice versa, we must use the sedimentary records in basins adjacent to these mountain ranges in order to reconstruct the long-term history of exhumation caused by erosion. Thermochronology measurements on bedrock currently exposed at the surface only provide constraints on the most recent stages of the cooling history of those particular units. By definition older bedrock has been removed so that the older erosional history can only be reconstructed through study of the sedimentary record. However, interpreting the sedimentary record can be complicated if burial of sediment resets sensitive low temperature thermochronometers, eliminating the cooling history of the source bedrocks (Carter 1999). Although higher temperature methods (e.g., muscovite Ar/Ar dating) (Szulc et al. 2006; White et

al. 2002) can be useful in examining past erosion and are resistant to resetting these have the disadvantage of being less sensitive to changes in the rates of exhumation by erosion because they require a greater amount of exhumation between isotopic closure and exposure at the surface. Nonetheless, detrital apatite fission track (AFT) can also have resolution problems, because single grain ages are often imprecise, especially for young grains with very low track counts.

A number of studies have examined the history of erosion in the Himalaya using the foreland basin sediment record, in particular sedimentary rocks belonging to the Miocene-Pliocene Siwalik Group (Baral et al. 2015; Bernet et al. 2006; Cerveny et al. 1989; Chirouze et al. 2015; Chirouze et al. 2013; Ghosh & Kumar 2000; Najman 2006; van der Beek et al. 2006). Although this stratigraphic unit has provided useful information about past patterns and rates of erosion the quality of information from AFT thermochronology has been limited due to resetting caused by post-deposition burial, especially in the lower parts of the section (van der Beek et al. 2006). In addition, the foreland basin sequence at any one particular location will typically reflect the rivers that are flowing from the Himalaya at that point, providing a localized record. Although this may be very useful for examining single rivers, it is often hard to judge how effective each sequence might be in reconstructing erosion at the regional scale. For example, because the trunk Indus River lies on the western edge of the drainage, Siwalik Group rocks in the eastern parts of the catchment provide no information about how its sediment load may have evolved.

In this study we present AFT data from new scientific boreholes in the western Indian Ocean in order to derive a regional image of changing erosion rates within the Western Himalayas since ca. 15.5 Ma, and in particular after 9 Ma. Use of the International Ocean

Discovery Program (IODP) boreholes in the Laxmi Basin (Fig. 1)(Pandey et al. 2016b) has the advantage that the sediment thickness is low (<1.1 km) and the geothermal gradient is 53˚C/km and 57˚C/km at Sites U1456 and U1457 respectively (Pandey et al. 2016b). Although these are high values this means that even the base of the section will fall below temperatures required to cause significant annealing or resetting of fission tracks in apatite, i.e. ~60–110˚C (Green 1989) and therefore the original cooling history of the bedrock sources will be preserved. All but one of the samples were recovered from depths shallower than 722 mbsf, implying no more than 38˚C burial temperature at the present maximum burial depth. The deepest sample (U1456E-19R-3, 10-20 cm) was recovered from a depth of 1103 mbsf but the fission track ages are older than the depositional age, indicating that this too is not reset.,

Constraining rates of bedrock source cooling caused by erosion driven by rock uplift can help identify locations of active tectonics and the rates and patterns of mountain growth. However, climate change may also play a role in relation to variations in precipitation rate that are linked to the intensity of the South Asian monsoon. This is known to have varied significantly throughout the Cenozoic (Betzler et al. 2016; Gupta et al. 2015; Kroon et al. 1991; Prell et al. 1992; Quade et al. 1989). Debate continues concerning the history of strengthening of the South Asian monsoon, but increasingly there is a consensus that the climate began to dry after 8 Ma (Behrensmeyer et al. 2007; Clift 2017; Singh et al. 2011), following a period of maximum intensity in the middle Miocene (Clift et al. 2008). It has been suggested that it is the strength of the summer monsoon rains during the middle Miocene that resulted in rapid exhumation of the Greater Himalaya at that time driven by strong erosion (Clift et al. 2008). If that is true one might predict that the rate of erosion since that time was also coupled with monsoon intensity. However, work within the foreland sedimentary rocks of the Siwalik Group

90 in Nepal shows that the rate of exhumation in the central Nepalese Himalaya remained
91 essentially constant after 8 Ma (van der Beek et al. 2006). In contrast, the same study argued that
92 rates of erosion had increased between 8 and 3 Ma in Western Nepal, despite the fact that both
93 sections lie within the Ganges drainage system, which is wetter than the Indus basin considered
94 here (Bookhagen & Burbank 2006). In contrast, AFT data from Ocean Drilling Program (ODP)
95 Sites 717 and 718 on the Bengal fan showed that rapid rates of exhumation of the bedrock
96 sediment sources to the Ganges-Brahmaputra basin has been ongoing since the middle Miocene
97 (Corrigan & Crowley 1990). Reappraisal of this data by van der Beek et al. (2006) indicated
98 relatively constant lag times (i.e., the difference between the depositional age and the AFT
99 cooling) since 9 Ma, suggestive of uniform erosion rates.
100 There are few constraints over how erosion rates might have changed during the
101 Pleistocene. While some have argued that the onset of northern hemisphere glaciation (NHG) has
102 intensified rates of erosion during the last couple of million years (Clift 2006; Métivier et al.
103 1999; Zhang et al. 2001), other workers, drawing on cosmogenic isotope data (Willenbring &
104 von Blanckenburg 2010), suggest that continental weathering rates have remained essentially
105 steady-state during the Neogene and especially the Plio-Pleistocene. Such an observation does
106 not require faster sediment delivery to the ocean, although this was proposed from a global data
107 compilation implying a steady state supply of sediment spanning tens of millions of years (Sadler
108 & Jerolmack 2014). Here we provide the first detailed AFT constraints on erosion rates in the
109 Western Himalaya, within the Indus basin, in order to see whether the temporal evolution in that
110 region mirrors that found in Nepal and in the Ganges-Brahmaputra drainage basin.
111 Over the period since 15.5 Ma considered by this study the Western Himalaya have
112 experienced significant tectonic changes. The Lesser Himalayas were brought to the surface

because of duplexing above the Main Boundary Thrust (MBT) (Huyghe et al. 2001; Mugnier et al. 1994), coupled with focused erosion since the Late Miocene. There is continued debate about when exposure of the Lesser Himalaya might have occurred. Early studies suggested that the MBT initiated around 10–11 Ma (Meigs et al. 1995) allowing the Lesser Himalayan Duplex to form and be uplifted and then eroded. Work from the Siwalik Group in Northwest India points to an initial exposure of the Lesser Himalaya at ca. 9 Ma followed by more widespread exposure after 6 Ma (Najman et al. 2009), although this may be only applicable to the Beas River area (Fig. 1). Nd and zircon U-Pb data from IODP Sites U1456 and U1457 now suggest initial exposure after 8.3 Ma and widespread unroofing after 1.9 Ma (Clift et al. 2019b). Other potentially important sources of sediment to the submarine fan include the Nanga Parbat massif that is located next to the Indus River in the Western Syntaxis (Fig. 1). Provenance studies from the Indus River downstream of Nanga Parbat indicate that this massif has only limited sediment generating potential at the present time (Clift et al. 2002b; Garzanti et al. 2005; Lee et al. 2003), despite the start of uplift ca. 6 Ma (Chirouze et al. 2015). In contrast, its eastern equivalent (Namche Barwe) is believed to be a major source of sediment to the Brahmaputra (Garzanti et al. 2004; Stewart et al. 2008). Bedrock thermochronology measurements testify to Nanga Parbat being very rapidly exhumed in the recent geologic past (Zeitler et al. 1993), but this does not seem to generate much of the sediment in the river downstream of that point (Alizai et al. 2011). Zircon fission track (ZFT) and Nd isotope data in the western part of the Siwalik ranges in Pakistan indicate that this massif and other Himalayan units in the western syntaxis may have become more important as a sediment source after around 6 Ma (Chirouze et al. 2015). The sedimentary record in the Indus Fan may also been affected by large-scale drainage capture. Neodymium isotope measurements on samples from an industrial drill site on the Indus shelf, as

136 well as limited ODP samples from the upper fan, were used to argue that the eastern tributaries
137 of the Indus River were only been captured into the modern system after 5 Ma (Clift & Blusztajn
138 2005). However, this is contradicted by combined ZFT and Nd isotope data that supports relative
139 stability in drainage patterns but changing rates of erosion in the Himalaya and Karakoram since
140 the Miocene (Chirouze et al. 2015).
141
142 **Regional Setting**
143 IODP Expedition 355 sampled sediments from the Indus Fan deposited within the Laxmi
144 Basin offshore western India (Fig. 1). Although the Laxmi Basin is separated from the main
145 Arabian Basin by the Laxmi Ridge, the bathymetry of the basin and the orientation of active
146 channels (Mishra et al. 2016) indicates that the primary source of sediment to the coring
147 locations would be the Indus River, with lesser input from peninsular rivers such as the Tapti and
148 Narmada. Initial petrographic-based interpretations of the sediments made shipboard during the
149 expedition suggested that there were limited amounts of sediment delivery from Western India,
150 and tend to be found only in the youngest parts of the section (Pandey et al. 2016a).
151 The Laxmi Basin itself dates from the latest Cretaceous when India began to separate from
152 the Seychelles (Bhattacharya et al. 1994; Pandey et al. 1995). Following the onset of India-Asia
153 collision, ca. 50–60 Ma (DeCelles et al. 2014; Najman et al. 2010), the uplift and erosion of the
154 Himalaya has resulted in a huge flux of sediment into the Arabian Sea. Although the Indus Fan is
155 much smaller than the Bengal Fan it is nonetheless the second largest sediment body on Earth
156 and is believed to have accumulated sediment eroded from the mountains at least since 45 Ma
157 (Clift et al. 2001).

158 Drilling during Expedition 355 recovered a section that penetrated to basement at Site
159 U1457 (Fig. 2), but because of large-scale mass wasting (Dailey et al. 2019) the most complete
160 erosional record only spans the last 10.8 m.y., with much of the older sediment either missing,
161 due to erosion or non-deposition, or not sampled. Coring was undertaken at two sites, Site U1456
162 in the central part of the Laxmi Basin, as well as at Site U1457 located on the flanks of the
163 Laxmi Ridge (Fig. 1). In general, the sediment at Site U1456 tended to be coarser grained (Fig.
164 2). The entire sedimentary cover is also more complete at Site U1456 than at Site U1457. The
165 coarse-grained, sandy sediment that forms the focus of this study was taken from both sites and
166 is the product of turbidity current flows. Nonetheless, significant parts of the section are fine-
167 grained muddy facies together with carbonate-rich intervals and these are interbedded with sandy
168 turbidite material caused by sedimentation on depositional lobes within the middle fan (Fig. 2).
169 There are also interbeds of calcareous-rich pelagic material that reflect times when the main
170 Indus-sourced depocentre was located to the west of the Laxmi Ridge, so that the primary clastic
171 flux from the Indus River was not reaching the drilling area. Because the drilling sites are located
172 above the carbonate compensation depth (CCD) it was possible to date the age of sedimentation
173 using a combination of nannofossil and foraminifera biostratigraphy coupled with
174 magnetostratigraphy that provides a relatively robust age model (Pandey et al. 2016b). Drilling
175 was able to penetrate a thick mass transport deposit (MTD) deposited just before 10.8 Ma
176 (Calvès et al. 2015), but at Site U1456 coring was able to recover a short interval below the
177 MTD, providing a single sample that is substantially older than any of the other sediments
178 recovered and which has been approximately dated at 15.5 Ma (Pandey et al. 2016a). At Site
179 U1457 all fan sediment predating the mass wasting event had been removed so that our studies
180 are restricted to the section younger than 10.8 Ma at that location.

We apply the AFT thermochronology dating method to this sediment in order to understand how the source rocks that provided material to the Arabian Sea evolved in their cooling and exhumation history since the middle Miocene. Fission track studies are a well-established method for looking at bedrock unroofing and potentially also sediment provenance if the source regions themselves are sufficiently well defined and if cooling ages are relatively constant in a source area (Carter 1999; Green et al. 1989; Laslett et al. 1987). In a complex area like the western Himalaya cooling ages vary across tectonic blocks and through time so that the interpretation of the AFT ages is contingent on supporting provenance data and cannot be used to constrain provenance by themselves. In this study we draw on zircon U-Pb age data from these same boreholes (Clift et al. 2019b). Simple comparison of modern bedrock AFT ages and detrital AFT ages in sediments more than around a million years old is not justifiable because the cooling rates of the bedrock will change on such timescales.

Methodology

Low-temperature AFT central ages reflect cooling through 60–125°C over time scales of 1–10 m.y. (Green et al. 1989). Fission tracks form continuously through time at an abundance determined by the concentration of ^{238}U in the host apatite grain (Haack 1977). The method has been a widely used and is effective for studying exhumation history and provenance of shallow-buried sediment (Carter 2007; Gallagher et al. 1995). Samples were taken where suitable sandy material was available at both IODP sites, as shown in Figure 2 and Table 1. Some of the apatites were extracted from the same samples analysed for detrital zircon U-Pb dating by Clift et al. (2019b).

Following mineral separation AFT analysis was performed at the London Geochronology Centre based at University College, London, UK. Polished grain mounts of apatite were etched with 5N HNO_3 at 20˚C for 20 seconds to reveal the spontaneous fission-tracks. Subsequently the uranium content of each crystal was determined by irradiation, which induced fission in a proportion of the ^{235}U. The induced tracks were registered in mica external detectors. The samples for this study were irradiated in the irradiated in the FRM 11 thermal neutron facility at the University of Munich, Germany. The neutron flux was monitored by including Corning glass dosimeter CN-5, with a known uranium content of 11 ppm, at either end of the sample stack. After irradiation, sample and dosimeter mica detectors were etched in 40% HF at 20˚C for 25 minutes. Only crystals with sections parallel to the c-crystallographic axis were counted, as these crystals have the lowest bulk etch rate. To avoid biased results through preferred selection of apatite crystals the samples were systematically scanned, and each crystal encountered with the correct orientation was analysed, irrespective of track density. The results of the fission track analysis are presented in Table 2 and online Supplementary Table 1. Because the chi test, used to detect extra Poisson variation, does not show how much over dispersion to be present in the dataset we include the central age and its percentage relative error because this provides a measure of the extent of age dispersion. It is also useful when there are low track counts (young ages) as the chi test is unreliable under these conditions.

Results

Because all samples showed evidence of over-dispersion we examined the range of single grain AFT ages in each sample using a combination of kernel density estimates (KDE) plots following the method of Vermeesch (2012) and the radial diagrams of Galbraith (1990)(Fig. 3).

Plots that combine both types of data presentation are known as abanico plots (Dietze et al. 2016). In the radial plots the single grain ages are plotted away from a central point on the left side of each diagram, with higher accuracy measurements plotted closer to the right-hand curved y-axis against which the ages are measured. This approach allows populations of grains with similar ages but varying degrees of uncertainty to be identified as arrays. In this particular study we focus on the identification of a minimum age population extracted using the algorithm of Galbraith (2005) that clusters in an array and trends towards the y-axis on the right-hand side of each diagram. This avoids problems associated with a general purpose, multi-component mixture model that can give a biased estimate of the minimum age towards younger values with increasing sample size. The radial plots show if there is a single source (single array) or multiple sources, if there are more than one array. Figure 3 and Table 2 show samples that have a second age component (P2) as defined by ten or more grains. In all cases the majority of analysed grains defines the minimum age and represents the time at which the dominant bedrock sources cooled through the AFT partial annealing zone (PAZ).

In each case we also show the calculated depositional age derived from the shipboard biostratigraphy and magnetic stratigraphy (Fig. 3). The minimum ages are older than or concordant with the depositional age, as might be expected in a relatively shallow borehole in which the temperatures are not elevated above those known to reset fission tracks in apatite crystals. All samples have minimum ages less than 20 Ma, and P2 AFT ages are all less than 40 Ma (apart from the youngest sample) post-dating the initial collision of India and Asia. There are particularly noteworthy concentrations of grain ages between 3 and 20 Ma. 50% of samples have a minimum age younger than 10 Ma. The minimum age gets younger with decreasing depositional age but not in a systematic way. The age difference between the minimum age and

249 deposition age is <5 m.y. for most samples, i.e., short lag times, but increases for samples
250 deposited between 7.84 and 8.2 Ma, as well as 7.07–7.28 Ma. The youngest sample (U1456A-
251 11H-6, 60-69 cm) is unlike many of the others in showing significantly older AFT ages (Fig. 3).

252 The youngest deposited sample is anomalous in having a minimum age population of
253 20.7 Ma, despite only having been deposited around 930 ka (Fig. 3A). This may be due to the
254 sample containing fewer apatites, with only 24 grains being countable, which is the smallest
255 number out of all samples analysed. This is in strong contrast with the much younger minimum
256 ages of the directly underlying samples. It is only the very oldest sample (~15 Ma, U1456E-19R-
257 3, 10–20 cm) which also has a minimum age of that value, but that sample has a short lag time
258 (Fig. 3W). We can assess the possible impact of low grain numbers on the critical minimum age
259 result in Figure 4. This plot shows that there is no correlation between the number of grains and
260 the minimum age, only reinforcing the fact that samples with low numbers of grains have more
261 uncertainty in the result, but not causing short lag times.

262 The core is not altered or veined and the modern maximum burial temperature of the
263 samples with lag times close to zero is far too cool to have affected the AFT ages. The ages are
264 within error of the depositional age, not resolvably younger. Although sample U1456D-12R-1
265 30-36 cm has a minimum age population slightly younger (6.6 ± 1.5 Ma) than the calculated
266 depositional age (7.0 Ma) but within error of that value and need not be reset. Moreover, the
267 young ages are also accompanied by older age populations that are also consistent with the
268 sediment not being thermally reset, as well as with the modern borehole temperatures being well
269 below the apatite partial annealing zone (556 mbsf (29.4˚C) at Site U1456, 572–590 mbsf (32.6–
270 33.6˚C) at Site U1457).

Discussion

The fact that all of our AFT ages are relatively young and mostly postdate widely accepted times of India-Asia collision is a clear indication that they are derived from Himalayan/Karakoram sources supplied by the Indus River and, with the exception of the youngest sample, not from peninsular India. Ancient rocks of the Indian peninsula have not been substantially deformed and uplifted during the Cenozoic and basement apatite fission track ages are mostly Jurassic-Cretaceous. Although they range as young as 54 Ma (Gunnell et al. 2003; Kalaswad et al. 1993), 95% of the ages measured are older than 100 Ma, averaging 228 Ma (Fig. 5H). This is somewhat older than most of the grain ages in Sample U1456A-11H-6, 60-69 cm., but does match the P2 older population in that sample (Table 2). Nonetheless, the minimum age population of 20.7±3.8 Ma requires a Himalaya-Karakoram provenance for 14 of the 24 grains measured. U-Pb zircon ages from this same sample (Clift et al. 2019b) show that 8.25% of the grains date to <200 Ma that require derivation from the Indus River because such zircon ages can only be generated by erosion from Kohistan or Karakoram sources. Zircon grains older than 300 Ma could be from the peninsula or the Himalaya. This youngest sample seems likely to be of mixed provenance, with material from both the Indus and the peninsula. For the other samples the AFT data argue strongly for the sand at these drilling sites being entirely derived from the Indus River because they are generally much younger than AFT ages from the western margin of peninsular India and broadly consistent with the AFT ages derived from sands that are definitely of Indus derivation (Clift et al. 2004; Clift et al. 2010).

Some information can also be derived about where the sediments may be coming from within the possible source ranges if we refer to the bedrock data that has been measured onshore, as summarized in Figure 5. Comparison of these sources and detrital data is only valid for the youngest sediments because young bedrock AFT ages do not inform us about the cooling of these sources in the older geologic past, only the cooling of the rocks now exposed. We note that the different ranges within the Indus basin have a number of distinctive peaks and that some of these are distinct in terms of their AFT age spectra. We note that the Greater and Lesser Himalaya have relatively similar fission track ages, clustering around 3–4 Ma, but with some ranging to ca. 1 Ma, at least in the Sutlej Valley (Thiede et al. 2004), and that these also overlap with ages known from the Karakoram, especially the eastern Karakoram (Wallis et al. 2016) and the Yasil Dome lying in the Karakoram immediately north of the Nanga Parbat Massif (Poupeau et al. 1991). The Karakoram however, also have bedrock AFT ages that range to older values, suggestive of earlier exhumation in at least parts of that block, most notably in the west and their continuation into the Hindu Kush (Zhuang et al. 2018). The very youngest grains are measured around the Nanga Parbat Massif (Zeitler 1985), while the oldest are found in the Transhimalayan Ladakh Batholith (Kirstein et al. 2009) and Deosai Plateau (van der Beek et al. 2009). The Tethyan Himalaya have also yielded older AFT ages in the central Himalaya (Li et al. 2015), but have not been dated within the Indus catchment. Uplift and erosion in the mountains around the Indus Suture and located to the north of the Greater Himalaya are widely accepted to have initiated earlier and then mostly slowed as the exhumation shifted into the Greater and Lesser Himalayan ranges (Searle, 1996).

Although many of the measured fission tracks at Nanga Parbat have ages of less than 1 Ma (Zeitler et al. 1989), clearly this could not have been the case before 1 Ma, when the fastest

cooled grains must have had ages within error of or older than 1 Ma. Lag times could however have been short prior to 1 Ma. Consequently, direct comparison of the modern bedrock with the detrital ages in old sediments is not appropriate for most of our samples. Because the cooling rates of bedrock sources change on timescale of $>10^6$ yr, not only would the AFT ages have been older in the past but we cannot assume that these sources still had the same lag times in the geologic past. Different, higher temperature thermochronometers can constrain exhumation rates during those earlier times and provide clues about lag times. We can however deduce that because many of the grains AFT ages are relatively young (<15 Ma) and their lag times are short that they were probably derived from fast exhuming sources in the Himalaya, Nanga Parbat or Karakoram (Zeitler et al. 1993; Zhuang et al. 2018), rather than in Kohistan, the Transhimalaya or Tethyan Himalaya where uplift and exhumation was mostly older. The cooling histories of these latter sources imply that their AFT lag times would be mostly long during the Late Miocene-Present (Fig. 5) (Kirstein et al. 2009; Krol et al. 1996; Searle 1996). Although some young AFT ages <6.3 Ma have been recorded in the Ladakh Transhimalayan Batholith along the Shyok Suture (Kirstein et al. 2009) these represent quite a small part of that tectonic block. Zircon U-Pb ages from the same IODP sites imply that the Transhimalaya has not been a dominant source during the period targeted by this study (maximum of 28% at 15.5 Ma and this is likely a large overestimate because the Karakoram and Transhimlaya overlap in zircon U-Pb ages) (Clift et al. 2019b).

The prevalence of short AFT lag times implies rapid exhumation in the dominant sediment-producing sources close to the time of sedimentation. The AFT data require that little sediment was stored for significant periods of geologic time between erosion in the mountain sources and sedimentation on the Indus submarine fan because the difference/lag between

minimum ages and deposition is typically <4 m.y. (75% of samples), representing an upper limit to the storage time. The lag time of a grain largely represents the time between cooling and erosion. While the lag time also includes time spent during sediment transport, study of the Quaternary Indus system indicates transport times of no more than ~10^5 y for the bulk of the sediment delivered to the deep basin (Clift & Giosan 2014). Some of the sediment may be recycled from foreland basin sedimentary rocks of the Siwalik Group and this would introduce an additional lag into the sediment transport history. Secondary AFT age populations between 15 and 38 Ma (Table 2) would fit with this type of recycling. We can discount that these older ages are coming from direct erosion of the slower cooled Ladakh Batholith or Tethyan Himalaya because heavy mineral studies (Garzanti et al. 2005), trace element characteristics of detrital amphiboles (Lee et al. 2003) and zircon U-Pb ages (Alizai et al. 2011) from the trunk Indus River close to the Himalayan front show dominance by the Karakoram (especially the Southern Karakoram Metamorphic Belt) over other sources in the modern upstream basin. That the Siwalik Group sedimentary rocks themselves have not been entirely reset in AFT during burial is known from studies in central Nepal (van der Beek et al. 2006) and these ranges could thus be a source of the older AFT ages measured. Quantifying the amount of recycling out of the Siwalik Ranges is impossible for our data because older grains could come from slow cooling sources or from the Siwalik Group. However, the high abundance of short lag time grains suggests that the degree of this recycling cannot be too large. Rates of incision in modern gorges cutting the Siwalik Group in Nepal have been used to estimate that they account for no more than 15% of the total flux (Lavé & Avouac 2001), while an isotope-based mass balance for the Ganges basin indicates <10% of the mass flux in that drainage is from the Siwalik Group (Wasson 2003). A contribution on that order to the Indus Basin would be consistent with the AFT data presented

here. The AFT data by themselves cannot resolve erosion from the Siwaliks, as they share older AFT ages with sources in the Tethyan Himalaya, Kohistan and Transhimalaya.

On shorter timescales if sediment was being buffered on the floodplains, in the delta or on the continental shelf then this is expected to have occurred only for a short amount of time, essentially tens of thousands of years (Li et al. 2019). Storage and recycling on million-year timescales would have resulted in longer lag times. When the lag times of our samples are 3–4 m.y. or some of this time must have been spent during transport. With the exception of storage and recycling via Siwalik Group foreland sequences discussed above the assumption is that most of this time would be spent prior to exposure and erosion because estimates of transport time in the Quaternary Indus are just 10^5 y for the bulk of the sediment delivered to the deep basin (Clift & Giosan 2014). Modern bedrock AFT data from the Greater and Lesser Himalaya and Karakoram indicate this order of lag time at the present day (Fig. 5), without factoring in much additional transport time. Our data are broadly consistent with the idea of rapidly uplifting mountains being strongly eroded and so supplying most of the sediment into the Indus River during the period of study since 15.5 Ma.

Combined Nd isotope and detrital zircon U-Pb age data from bulk sediment samples from Sites U1456 and U1457 show that there was a change in provenance starting around 5.7 Ma (Clift et al. 2019b). This analysis indicates more material coming from the Greater and Lesser Himalaya and relatively less from the Karakoram after this time. The range of lag times in sediments younger than 7.0 Ma is similar to those found at the Indus delta during the phase of strong summer monsoon in the early Holocene, i.e. 2–5 m.y. (Fig. 6), when the provenance constraints indicates that these were preferentially derived from Greater and Lesser Himalayan sources (Clift et al. 2019b). In contrast, sediments older than 7.0 Ma have longer lag times (3.5–

384 8.8 m.y., average 6.0 m.y.) and are inferred to be more derived from the Karakoram, based on
385 their zircon U-Pb age spectra (Fig. 6) (Clift et al. 2019b). The fact that lag times of pre-7.0 Ma
386 samples are longer, like Indus Delta LGM sediments that have an AFT central age of 9 ± 1 Ma
387 (Clift et al. 2010) is consistent with a dominant Karakoram source.

388 That the Nd isotope provenance data change at around the same time as the AFT lag
389 times (after 5.7 Ma; Fig. 6) supports the idea that a change in provenance may account for at
390 least part of the changing AFT lag times at that time. The absence of the very short lag time
391 samples does mean that after 5.7 Ma there are no longer any significant fast eroding ranges in the
392 catchment. As noted above, the Crystalline Inner Lesser Himalaya are known to be experiencing
393 unroofing after ~6 Ma, at least in the vicinity of the Beas River catchment (Najman et al. 2009)
394 and the shift in the general character of the AFT age populations after 5.7 Ma may in large part
395 simply reflect more sediment delivery from the Greater and Lesser Himalayas, potentially related
396 to tectonic imbrication and rock uplift (Bollinger et al. 2004; Huyghe et al. 2001; Webb 2013).
397 Such a shift is consistent with the evolving provenance data in Laxmi Basin (Clift et al. 2019b).
398 The structural reconstructions of Webb (2013) for the western Himalaya propose that both the
399 Greater and Lesser Himalaya remained buried under the Tethyan Himalaya until after 5.4 Ma.
400 This would imply that the source of rapidly cooled grains before that time would be from the
401 Karakoram and Tethyan Himalaya.

402 The AFT ages can be used to constrain changing rates of exhumation in the bedrock
403 sources. Comparing depositional age against the AFT minimum age populations allows us to
404 assess the lag time between cooling of bedrock sources as they passed through the 60–110˚C
405 partial annealing zone and their final deposition in the deep water of the Indian Ocean (Fig. 6). In
406 our analysis we further compare our results with those similar aged fluvial sedimentary rocks

from the Siwalik Group in Western and Central Nepal (van der Beek et al. 2006), as well as from the Bengal Fan collected by ODP Leg 116 (Corrigan & Crowley 1990). It is clear that many of these minimum age groups have relatively short lag times, which indicates fast cooling and exhumation of bedrock sources. We note that both the oldest (15.5 Ma) sample from the Laxmi Basin and a slightly younger sample from the Bengal Fan show lag times close to 4 m.y. in the middle Miocene. This would imply exhumation rates of 1.1–1.4 km/m.y. assuming 25–35˚C/km geothermal gradients.

Unfortunately, we have little information between that time and ~8.5 Ma when the next youngest dateable sandy sediment was deposited and preserved at the drilling sites. Although one of the minimum age groups still lags by ~4.2 m.y., we note that this there is some scatter to longer lag times of up to 8.8 m.y. between 8.5 and 7.0 Ma and with large uncertainties. Combined zircon U-Pb (40–70 and 70–120 Ma grains) and bulk sediment Nd isotope (ε_{Nd} values > -10) provenance data indicate that much of the sediment at that time was derived from the Karakoram (Clift et al. 2019b). The zircon U-Pb budget over-represents the net flux from the Himalaya because these bedrocks are >2.2 time more fertile with regard to zircon than the Karakoram and Transhimalaya.

After 7.0 Ma lag times shortened significantly. Three samples from the Laxmi Basin drilling sites are within error of the depositional age between 7.0 and 5.7 Ma, requiring exhumation rates that were so rapid that we are unable to constrain the duration between cooling through the PAZ (60–110˚C) and sedimentation, i.e., lag times close to zero. This implies a maximum rate of cooling in the sources at that time. All three of the fast cooling samples have accompanying zircon U-Pb ages that show that they continue a trend towards more Himalayan erosion but that there is not a sharp contrast with the sediment deposited before 7.0 Ma. After 5.7

Ma the change in Nd isotopes is especially marked implies that a change in provenance may be responsible for the slowing of exhumation rates. Nonetheless, one sample, U1457C-43R-1 55-63 cm, deposited at 5.78 Ma, has a minimum age lag time 3.13 m.y., longer than the others. This implies that not all sources were supplying large volumes of sediment at all times and that not all bedrock sources were exhuming so quickly.

Although provenance data indicate mostly Karakoram sources, these rapidly cooled grains could also be derived from the Himalaya. Zircon U-Pb ages allow us to discriminate between erosion of Karakoram (40–120 Ma and Himalayan (>300 Ma) sources but we only know that these are the largest sources at that time. However, the zircon ages only apply to these minerals and the provenance cannot be transferred to the apatites so that we only know that there were rapidly cooling areas between 7.0 and 5.7 Ma but not which range they are located in. However, because there are large numbers of grains in the minimum age group it might reasonably be expected that these are derived from bedrocks sources that also supply large volumes of other mineral types. Between 7.0 and 5.7 Ma the longest lag time was 3.13 m.y. in the sediment deposited at 5.87 Ma. This indicates an average cooling rate of at least 35.1±9.7˚C/m.y., faster than the cooling rates of 12.5 to 26.1˚C/m.y. between 8.2 and 7.0 Ma. These are faster rates than those recorded in the Siwalik Group from Nepal (van der Beek et al. 2006), as well as sparse data from the Bengal Fan (Corrigan & Crowley 1990), although they are within the uncertainties of the peak rates in Nepal at that time. However, in Nepal the sources must have been Himalayan, not Karakoram. In the youngest part of the section (<4 Ma), which is more dominated by Himalaya erosion (Clift et al. 2019b) these very short lag times are not visible and are always more than 1.93 m.y., equivalent to approximate exhumation rates of ~2.3–1.6 km/m.y. The moderate exhumation rates after 4 Ma compare with data from both the Bengal

453 Fan and from the Nepalese part of the Himalayan foreland. Both these sediment sequences are
454 dominated by Himalayan erosion (Bouquillon et al. 1990). Slowing of exhumation in the Indus
455 basin after 5.7 Ma is consistent with data from western Nepal (Karnali), but the slowing from
456 peak rates at 7.0 to 5.7 Ma is in contrast to conclusions of work from central Nepal (Surai and
457 Tinau Khola) that argued for relatively steady state cooling in that part of the mountain range
458 (van der Beek et al. 2006). The very youngest sample deposited at 930 ka stands out as having by
459 far the largest lag time and is inferred have a unique source, likely a mixture of sediment from
460 the Indus River and Peninsular India.

461 We can compare this pattern of accelerating exhumation before 7.0 Ma and then slowing
462 after 5.7 Ma with the climatic history (Fig. 6), while recognizing the shift in provenance that is
463 occurring at the same time. One of the most popular long-term proxies for monsoon intensity in
464 the Arabian Sea is the relative abundance of *G Bulloides* offshore the margin of Arabia. The
465 abundance of *G. Bulloides* is largely a function of the availability of nutrients derived from
466 upwelling caused by the summer monsoon rains (Curry et al. 1992). There is little evidence for
467 such strong upwelling prior to around 13 Ma (Betzler et al. 2016). A general intensification of
468 upwelling is noted after 5.3 and 3.0 Ma (Gupta et al. 2015; Huang et al. 2007) (Fig. 6). However,
469 upwelling is not a direct proxy of rainfall and this apparent intensification does not reflect the
470 delivery of summer rains to the mountain front, because this proxy does not correlate with other
471 climatically sensitive indicators (Clift 2017).

472 Stable oxygen isotope data from the foreland basin instead agree with chemical
473 weathering data from the South China and Arabian Seas in arguing for relatively wet conditions
474 in the middle Miocene between 10 and 12 Ma (Dettman et al. 2001), followed by a decrease in
475 humidity particularly after around 6–8 Ma (Clift 2017; Singh et al. 2011). Moisture delivery to

this area from the winter Westerlies is also reconstructed to reduce around 7 Ma (Vögeli et al. 2017). The increasing lag time seen in the minimum age populations after 5.7 Ma would be consistent with slower erosion and could be linked to weaker monsoon rainfall. Weaker monsoon and Westerly rains would also reduce discharge and potentially slow the transport of sediment across the flood plains. Increased aridity is consistent with decreasing strength of chemical weathering seen in Indus Marine A-1 located on the Indus shelf (Clift et al. 2008), as well as Site U1456 (Clift et al. 2019a), but largely postdates the carbon isotope transition from 8 to 6 Ma in the foreland basin (Quade et al. 1989).

The acceleration in exhumation rates from 7.8 to 7.0 Ma generally coincides with the climatic drying, which may seem counterintuitive. However, this also assumes that stronger rains, sometimes modulated through glaciation, always increase erosion. There is evidence that drier conditions, especially when this involves heightened seasonality, can increase erosion provided the drying is not too extreme, but sufficient to reduce vegetation cover that reduces soil erosion (Giosan et al. 2017). There is no evidence that the period of fast erosion at 5.7–7.0 Ma was caused by faster India and Asia convergence. Indeed, convergence rates appear to have slowed gradually during the Cenozoic (Clark 2012).

Conclusions

Apatite fission track ages derived from turbidite sediments from IODP Sites U1456 and U1457 in the Laxmi Basin, eastern Arabian Sea, provide an opportunity to reconstruct changing exhumation rates in the western Himalaya and Karakoram since 15.5 Ma, and especially since 9 Ma. AFT ages are mostly <50 Ma and demonstrate that the sediment is derived from the Indus

498 River, not peninsular India, except in the case of the youngest sample, deposited at 0.93 Ma.
499 Moreover, most samples show minimum age populations that are only slightly older than the
500 depositional age, implying fast rates of exhumation in the sources through this time. Lag times of
501 ~4 m.y. in the Middle Miocene imply exhumation rates of 1.1–1.4 km/m.y. After a period of
502 longer lag times (~6 m.y.) between 8.5 and 7.8 Ma these reach a minimum from 7.0 to 5.7 Ma,
503 when lag times were within error of zero. Provenance U-Pb zircon and Nd isotope data indicate
504 erosion dominantly in the Karakoram, but the AFT ages could have also come from Himalayan
505 sources, which were also important contributors at this time. The AFT data alone do not allow us
506 to discriminate which of the two ranges contained the fast exhuming sources. After 5.7 Ma lag
507 times lengthened to ~4.5 Ma, and exhumation rates slowed to 2.3–1.6 km/m.y. at the same time
508 that sediment supply came progressively more from the Himalaya and relatively less from the
509 Karakoram.

510 The time of peak exhumation correlates with the transition to a drier climate in the
511 foreland basin and of a weakening Westerly Jet. Erosion rates since 5.7 Ma are comparable or
512 slightly faster than those seen in the Nepalese parts of the Himalaya and the Bengal Fan. Slowing
513 exhumation rates after 5.7 Ma correlate with a drying climate and weaker summer monsoon rains
514 in the Late Miocene. There is a general shift in the AFT age populations from longer lag times,
515 more similar to the glacial era Indus River and associated with dominant erosion in the
516 Karakoram prior to 7 Ma, to shorter lag times and more erosion of the Himalaya, similar to the
517 Holocene Indus River after 5.7 Ma. The acceleration of exhumation as the climate dried between
518 7.8 and 7.0 Ma seems to imply a dominant tectonic control of erosion. The AFT data support
519 models that imply a non-linear relationship between summer monsoon rain strength and the
520 erosion of the western Himalaya.

Acknowledgements

This research used samples and/or data provided by the International Ocean Discovery Program (IODP). Funding for this research was provided by USSSP and the Charles T. McCord Jr Chair in Petroleum Geology at LSU. We thank GeoSep Services and especially Paul O'Sullivan for separation of our apatite grains. The paper was improved by reviews from Peter van der Beek and an anonymous reviewer.

530 **Figure Captions**

531

532 Figure 1. Shaded bathymetric and topographic map of the Arabian Sea area showing the location
533 of the drilling sites within the Laxmi Basin. Map also shows the primary source ranges and the
534 major tributary systems of the Indus River, as well as smaller peninsular Indian rivers that may
535 have provided material to the drill sites. Magnetic anomalies are from Miles et al. (1993). KK =
536 Karakoram; NP = Nanga Parbat; K = Karnali; S = Surai Khola; T = Tinau Khola.

537

538 Figure 2. Simplified lithologic logs of the two drill sites considered in this study. Black arrows
539 show the location of the samples analysed. MTD = Mass Transport Deposit.

540

541 Figure 3. Radial plots and associated KDE spectra (abanico plots) showing the range of apatite
542 fission track ages for each of the samples considered within the study (Galbraith 1990). Ns—
543 number of spontaneous fission tracks; Ni—number of induced tracks. Single ages are plotted
544 with standard errors according to their precision ($1/\sigma$ on the 'x' axis). The error attached to each
545 plotted point is standardized on the y scale. The value of the age and the 2σ uncertainty can be
546 read off the radial axis by extrapolating lines from point 0,0 through the plotted age.

547

548 Figure 4. Cross plot of numbers of grains compared to minimum ages with 2σ uncertainties
549 displayed. There is no correspondence between the numbers of grains and the minimum age that
550 might bias the result of the lag time analysis.

551

552 Figure 5. KDE plots for the apatite fission track central ages of potential bedrock sources within
553 the headwaters of the Indus basin. Nanga Parbat data are from Warner et al. (1993), and Zeitler
554 (1985). Greater Himalaya data are from Kumar et al. (1995), Jain et al. (2000) and Thiede et al.
555 (2004). Lesser Himalaya data are from Thiede et al. (2004) and Vannay et al. (2004). Karakoram
556 data are from Foster et al. (1994), Zeitler (1985), Wallis et al. (2016) and Poupeau et al. (1991).
557 Kohistan data are from Zeitler (1985) and Zeilinger et al. (2001). Transhimalaya data are from
558 Kirstein et al. (2009; 2006), and Clift et al. (2002a). Tethyan Himalaya data are from Li et al.
559 (2015) and unpublished from Andrew Carter (UCL, 2017). Indian Peninsula data are from
560 Gunnell et al. (2003) and Kalaswad et al. (1993).

561

562 Figure 6. Lag time plot of detrital apatite fission track minimum ages showing the lag time
563 between the cooling and depositional ages. Note the minimum lag time achieved between 9 and
564 6 Ma. Siwalik data from Nepal is from van der Beek et al. (2006), Bengal Fan data is from
565 Corrigan and Crowley (1990). Monsoon records of *G. Bulloides* from Huang et al. (2007),
566 foreland basin $\delta^{14}C$ record from Quade et al. (1989). Sediment budget for Indus Fan from Clift
567 (2006). Evolution in the age spectra of zircon U-Pb ages and ε_{Nd} values is from Clift et al.
568 (2019b). Stippled area shows the time of the climatic transition to drier conditions in the foreland
569 basin.

570

571 Table 1. List of the samples with their depths and calculated depositional ages. Those samples
572 also analysed for detrital U-Pb zircon dating by Clift et al. (2019b) are highlighted.

573

574 Table 2. Summary of apatite fission track analytical data. Track densities are ($x10^6$ tr cm^{-2})
575 numbers of tracks counted (N) shown in brackets. Analyses by external detector method using
576 0.5 for the $4\pi/2\ \pi$ geometry correction factor. Ages calculated using dosimeter glass CN-5;
577 (apatite) ζ_{CN5} =338±5; calibrated by multiple analyses of IUGS apatite and zircon age standards
578 (Hurford 1990). $P\chi^2$ is probability for obtaining χ^2 value for v degrees of freedom, where v = no.
579 crystals – 1. Central age is a modal age, weighted for different precisions of individual crystals
580 (see Galbraith (1990)). Minimum age model after Galbraith (2005). P2 used peak fitting
581 algorithm of Galbraith and Green (1990) where there are > 10 grains.

582

583 Supplementary Table 1. Single grain apatite fission track data.

584

585

References

ALIZAI, A., CARTER, A., CLIFT, P. D., VANLANINGHAM, S., WILLIAMS, J. C. & KUMAR, R. 2011. Sediment provenance, reworking and transport processes in the Indus River by U-Pb dating of detrital zircon grains. *Global and Planetary Change* 76, 33-55, doi:10.1016/j.gloplacha.2010.11.008.

BARAL, U., LIN, D. & CHAMLAGAIN, D. 2015. Detrital zircon U–Pb geochronology of the Siwalik Group of the Nepal Himalaya: implications for provenance analysis. *International Journal of Earth Science*, 1-19, doi;10.1007/s00531-015-1198-7.

BEHRENSMEYER, A. K., QUADE, J., CERLING, T. E., KAPPELMAN, J., KHAN, I. A., COPELAND, P., ROE, L., HICKS, J., STUBBLEFIELD, P., WILLIS, B. J. & LATORRE, C. 2007. The structure and rate of late Miocene expansion of C4 plants: Evidence from lateral variation in stable isotopes in paleosols of the Siwalik Group, northern Pakistan. *Geological Society of America Bulletin* 119(11/12), 1486-505., doi: 10.1130/B26064.1.

BERNET, M., VAN DER BEEK, P., PIK, R., HUYGHE, P., MUGNIER, J.-L., LABRIN, E. & SZULC, A. G. 2006. Miocene to Recent exhumation of the central Himalaya determined from combined detrital zircon fission-track and U/Pb analysis of Siwalik sediments, western Nepal. *Basin Research* 18, 393–412, doi: 10.1111/j.1365-2117.2006.00303.

BETZLER, C., EBERLI, G. P., KROON, D., WRIGHT, J. D., SWART, P. K., NATH, B. N., ALVAREZ-ZARIKIAN, C. A., ALONSO-GARCÍA, M., BIALIK, O. M., BLÄTTLER, C. L., GUO, J. A., HAFFEN, S., HOROZAI, S., INOUE, M., JOVANE, L., LANCI, L., LAYA, J. C., MEE, A. L. H., LÜDMANN, T., NAKAKUNI, M., NIINO, K., PETRUNY, L. M., PRATIWI, S. D., REIJMER, J. J. G., REOLID, J., SLAGLE, A. L., SLOSS, C. R., SU, X., YAO, Z. & YOUNG, J. R. 2016. The abrupt onset of the modern South Asian Monsoon winds. *Scientific Reports* 29838, doi:10.1038/srep29838.

BHATTACHARYA, G. C. B., CHAUBEY, A. K., MURTY, G. P. S., SRINIVAS, S., SARMA, K. V., SUBRAHMANYAM, V. & KRISHNA, K. S. 1994. Evidence for seafoor spreading in the Laxmi Basin, northeastern Indian Ocean. *Earth and Planetary Science Letters* 125, 211-20.

BOLLINGER, L., AVOUAC, J. P., BEYSSAC, O., CATLOS, E. J., HARRISON, T. M., GROVE, M., GOFFE, B. & SAPKOTA, S. 2004. Thermal structure and exhumation history of the Lesser Himalaya in central Nepal. *Tectonics* 23(5), 19, doi:10.1029/2003TC001564.

BOOKHAGEN, B. & BURBANK, D. W. 2006. Topography, relief, and TRMM-derived rainfall variations along the Himalaya. *Geophysical Research Letters* 33(L08405), doi:10.1029/2006GL026037.

BOUQUILLON, A., FRANCE-LANORD, C., MICHARD, A. & TIERCELIN, J. 1990. Sedimentology and isotopic chemistry of the Bengal Fan sediments: the denudation of the Himalaya. In *Proceedings of the Ocean Drilling Program, Scientific Results* eds J. R. Cochran, D. A. V. Stow and C. Auroux). pp. 43-58. College Station, TX: Ocean Drilling Program. 116, 43-58.

CALVÈS, G., HUUSE, M., CLIFT, P. D. & BRUSSET, S. 2015. Giant fossil mass wasting off the coast of West India: The Nataraja submarine slide. *Earth and Planetary Science Letters* 432, 265–72, doi:10.1016/j.epsl.2015.10.022.

CARTER, A. 1999. Present status and future avenues of source region discrimination and characterization using fission track analysis. *Sedimentary Geology* 124(1), 31-45, doi:10.1016/S0037-0738(98)00119-5.

CARTER, A. 2007. Heavy minerals and detrital fission-track thermochronology. *Developments in Sedimentology* 58, 851-68, doi:10.1016/S0070-4571(07)58033-7.
CERVENY, P. F., JOHNSON, N. M., TAHIRKHELI, R. A. K. & BONIS, N. R. 1989. Tectonic and geomorphic implications of Siwalik Group heavy minerals, Potwar Plateau, Pakistan. In *Tectonics of the Western Himalayas* eds L. L. Malinconico and R. J. Lillie). pp. 129–36. Boulder, Colorado: Geological Society of America Special Paper, 232, 129–36.
CHIROUZE, F., HUYGHE, P., CHAUVEL, C., VAN DER BEEK, P., BERNET, M. & MUGNIER, J.-L. 2015. Stable Drainage Pattern and Variable Exhumation in the Western Himalaya since the Middle Miocene. *Journal of Geology* 123, 1–20, doi:10.1086/679305.
CHIROUZE, F., HUYGHE, P., VAN DER BEEK, P., CHAUVEL, C., CHAKRABORTY, T., DUPONT-NIVET, G. & BERNET, M. 2013. Tectonics, exhumation, and drainage evolution of the eastern Himalaya since 13 Ma from detrital geochemistry and thermochronology, Kameng River Section, Arunachal Pradesh. *Geological Society of America Bulletin* 125(3-4), 523-38.
CLARK, M. K. 2012. Continental collision slowing due to viscous mantle lithosphere rather than topography. *Nature* 483, 74-77, doi:10.1038/nature10848.
CLIFT, P. D. 2006. Controls on the erosion of Cenozoic Asia and the flux of clastic sediment to the ocean. *Earth and Planetary Science Letters* 241(3-4), 571-80.
CLIFT, P. D. 2017. Cenozoic sedimentary records of climate-tectonic coupling in the Western Himalaya. *Progress in Earth and Planetary Science* 4(39), 1-22, doi:10.1186/s40645-017-0151-8.
CLIFT, P. D. & BLUSZTAJN, J. S. 2005. Reorganization of the western Himalayan river system after five million years ago. *Nature* 438(7070), 1001-03.
CLIFT, P. D., CAMPBELL, I. H., PRINGLE, M. S., CARTER, A., ZHANG, X., HODGES, K. V., KHAN, A. A. & ALLEN, C. M. 2004. Thermochronology of the modern Indus River bedload; new insight into the control on the marine stratigraphic record. *Tectonics* 23(TC5013), doi:10.1029/2003TC001559.
CLIFT, P. D., CARTER, A., KROL, M. & KIRBY, E. 2002a. Constraints on India; Eurasia collision in the Arabian Sea region taken from the Indus Group, Ladakh Himalaya, India. In *The tectonic and climatic evolution of the Arabian Sea region* eds P. D. Clift, D. Kroon, C. Gaedicke and J. Craig). pp. 97-116. London: Geological Society. Special Publications, 195, 97-116.
CLIFT, P. D. & GIOSAN, L. 2014. Sediment fluxes and buffering in the post-glacial Indus Basin. *Basin Research* 26, 369–86, doi:10.1111/bre.12038.
CLIFT, P. D., GIOSAN, L., CARTER, A., GARZANTI, E., GALY, V., TABREZ, A. R., PRINGLE, M., CAMPBELL, I. H., FRANCE-LANORD, C., BLUSZTAJN, J., ALLEN, C., ALIZAI, A., LÜCKGE, A., DANISH, M. & RABBANI, M. M. 2010. Monsoon control over erosion patterns in the Western Himalaya: possible feed-backs into the tectonic evolution. In *Monsoon evolution and tectonic-climate linkage in Asia* eds P. D. Clift, R. Tada and H. Zheng). pp. 181–213. London: Geological Society. Special Publication, 342, 181–213.
CLIFT, P. D., HODGES, K., HESLOP, D., HANNIGAN, R., HOANG, L. V. & CALVES, G. 2008. Greater Himalayan exhumation triggered by Early Miocene monsoon intensification. *Nature Geoscience* 1, 875-80, doi:10.1038/ngeo351.
CLIFT, P. D., KULHANEK, D. K., ZHOU, P., BOWEN, M. G., VINCENT, S. M., LYLE, M. & HAHN, A. 2019a. Chemical Weathering and Erosion Responses to Changing Monsoon Climate in the Late Miocene of Southwest Asia. *Geological Magazine*, doi:10.1017/S0016756819000608.

675 CLIFT, P. D., LEE, J. I., HILDEBRAND, P., SHIMIZU, N., LAYNE, G. D., BLUSZTAJN, J., BLUM, J. D.,
676 GARZANTI, E. & KHAN, A. A. 2002b. Nd and Pb isotope variability in the Indus River
677 system; implications for sediment provenance and crustal heterogeneity in the western
678 Himalaya. *Earth and Planetary Science Letters* 200(1-2), 91-106, doi:10.1016/S0012-
679 821X(02)00620-9.
680 CLIFT, P. D., SHIMIZU, N., LAYNE, G., GAEDICKE, C., SCHLÜTER, H. U., CLARK, M. K. & AMJAD,
681 S. 2001. Development of the Indus Fan and its significance for the erosional history of the
682 western Himalaya and Karakoram. *Geological Society of America Bulletin* 113, 1039–51.
683 CLIFT, P. D., ZHOU, P., STOCKLI, D. F. & BLUSZTAJN, J. 2019b. Regional Pliocene Exhumation of
684 the Lesser Himalaya in the Indus Drainage. *Solid Earth* 10, 647–61, doi:10.5194/se-10-
685 647-2019.
686 CORRIGAN, J. D. & CROWLEY, J. L. 1990. Fission track analysis of detrital apatites from Sites 717
687 and 718, leg 116, central Indian Ocean. *Proceedings of the Ocean Drilling Program,*
688 *Scientific Results* 116, 75–92.
689 CURRY, W. B., OSTERMANN, D. R., GUPTHA, M. V. S. & ITEKKOT, V. 1992. Foraminiferal
690 production and monsoonal upwelling in the Arabian Sea; evidence from sediment traps. In
691 *Upwelling systems; evolution since the early Miocene* eds C. P. Summerhayes, W. L. Prell
692 and K. C. Emeis). pp. 93–106. London: Geological Society. Special Publication, 64, 93–
693 106.
694 DAILEY, S. K., CLIFT, P. D., KULHANEK, D. K., BLUSZTAJN, J., ROUTLEDGE, C. M., CALVÈS, G.,
695 O'SULLIVAN, P., JONELL, T. N., PANDEY, D. K., ANDÒ, S., COLETTI, G., ZHOU, P., LI, Y.,
696 NEUBECK, N. E., BENDLE, J. A. P., BRATENKOV, S., GRIFFITH, E. M., GURUMURTHY, G. P.,
697 HAHN, A., IWAI, M., KHIM, B.-K., KUMAR, A., KUMAR, A. G., LIDDY, H. M., LU, H., LYLE,
698 M. W., MISHRA, R., RADHAKRISHNA, T., SARASWAT, R., SAXENA, R., SCARDIA, G.,
699 SHARMA, G. K., SINGH, A. D., STEINKE, S., SUZUKI, K., TAUXE, L., TIWARI, M., XU, Z. &
700 YU, Z. 2019. Large-scale Mass Wasting on the Miocene Continental Margin of Western
701 India. *Geological Society of America Bulletin*, doi:/10.1130/B35158.1.
702 DECELLES, P. G., KAPP, P., GEHRELS, G. E. & DING, L. 2014. Paleocene-Eocene foreland basin
703 evolution in the Himalaya of southern Tibet and Nepal: Implications for the age of initial
704 India-Asia collision. *Tectonics* 33, 824–49, doi:10.1002/ 2014TC003522.
705 DETTMAN, D. L., KOHN, M. J., QUADE, J., RYERSON, F. J., OJHA, T. P. & HAMIDULLAH, S. 2001.
706 Seasonal stable isotope evidence for a strong Asian monsoon throughout the past 10.7 m.y.
707 *Geology* 29(1), 31-34.
708 DIETZE, M., KREUTZER, S., BUROW, C., FUCHS, M. C., FISCHER, M. & SCHMIDT, C. 2016. The
709 abanico plot: Visualising chronometric data with individual standard errors. *Quaternary*
710 *Geochronology* 31, 12-18, doi:10.1016/j.quageo.2015.09.003.
711 FOSTER, D. A., GLEADOW, A. J. W. & MORTIMER, G. 1994. Rapid Pliocene exhumation in the
712 Karakoram (Pakistan), revealed by fission-track thermochronology of the K2 gneiss.
713 *Geology* 22(1), 19-22.
714 GALBRAITH, R. F. 1990. The radial plot: Graphical assessment of spread in ages *Nuclear Tracks*
715 *and Radiation Measurement* 17, 207–14.
716 GALBRAITH, R. F. 2005. *Statistics for fission track analysis*. CRC Press.
717 GALBRAITH, R. F. & GREEN, P. F. 1990. Estimating the component ages in a finite mixture.
718 *Nuclear Tracks and Radiation Measurement* 17, 197-206.

GALLAGHER, K., HAWKESWORTH, C. J. & MANTOVANI, M. S. M. 1995. Denudation, fission track analysis and the long-term evolution of passive margin topography: application to the S.E. Brazilian margin. *Journal of South American Earth Sciences* 8, 65-77.

GARZANTI, E., VEZZOLI, G., ANDO, S., FRANCE-LANORD, C., SINGH, S. K. & FOSTER, G. 2004. Sand petrology and focused erosion in collision orogens: the Brahmaputra case. *Earth and Planetary Science Letters* 220(1-2), 157-74.

GARZANTI, E., VEZZOLI, G., ANDO, S., PAPARELLA, P. & CLIFT, P. D. 2005. Petrology of Indus River sands; a key to interpret erosion history of the western Himalayan syntaxis. *Earth and Planetary Science Letters* 229(3-4), 287-302, doi: 10.1016/j.epsl.2004.11.008.

GHOSH, S. K. & KUMAR, R. 2000. Petrography of Neogene Siwalik sandstone of the Himalayan foreland basin, Garhwal Himalaya: Implications for source area tectonics and climate. *Journal of the Geological Society of India* 55, 1-15.

GIOSAN, L., PONTON, C., USMAN, M., BLUSZTAJN, J., FULLER, D. Q., GALY, V., HAGHIPOUR, N., JOHNSON, J. E., MCINTYRE, C., WACKER, L. & EGLINTON, T. I. 2017. Short communication: Massive erosion in monsoonal central India linked to late Holocene land cover degradation. *Earth Surface Dynamics* 5, 781-89, doi:10.5194/esurf-5-781-2017.

GREEN, P. F. 1989. Thermal and tectonic history of the East Midlands shelf (onshore UK) and surrounding regions assessed by apatite fission track analysis. *Journal of the Geological Society* 146, 755-73.

GREEN, P. F., DUDDY, I. R., LASLETT, G. M., HEGARTY, K. A., GLEADOW, A. J. W. & LOVERING, J. F. 1989. Thermal annealing of fission tracks in apatite; 4, Quantitative modelling techniques and extension to geological timescales. *Chemical Geology; Isotope Geoscience Section* 79(2), 155-82.

GUNNELL, Y., GALLAGHER, K., CARTER, A., WIDDOWSON, M. & HURFORD, A. J. 2003. Denudation history of the continental margin of western peninsular India since early Mesozoic—reconciling apatite fission track data with geomorphology. *Earth and Planetary Science Letters* 215(1-2), 187-201.

GUPTA, A. K., YUVARAJA, A., PRAKASAM, M., CLEMENS, S. C. & VELU, A. 2015. Evolution of the South Asian monsoon wind system since the late Middle Miocene. *Palaeogeography, Palaeoclimatology, Palaeoecology* 438, 160–67, doi:10.1016/j.palaeo.2015.08.006.

HAACK, U. 1977. The closing temperature for fission track retention in minerals. *American Journal of Science* 277, 459-64.

HUANG, Y., CLEMENS, S. C., LIU, W., WANG, Y. & PRELL, W. L. 2007. Large-scale hydrological change drove the late Miocene C4 plant expansion in the Himalayan foreland and Arabian Peninsula. *Geology* 35(6), 531-34.

HURFORD, A. 1990. Standardization of fission track dating calibration: Recommendation by the Fission Track Working Group of the IUGS subcommission on geochronology. *Chemical Geology* 80, 177–78.

HUYGHE, P., GALY, A., MUGNIER, J.-L. & FRANCE-LANORD, C. 2001. Propagation of the thrust system and erosion in the Lesser Himalaya: Geochemical and sedimentological evidence. *Geology* 29(11), 1007–10.

JAIN, A. K., KUMAR, D., SINGH, S., KUMAR, A. & LAL, N. 2000. Timing, quantification and tectonic modelling of Pliocene-Quaternary movements in the NW Himalaya; evidence from fission track dating. *Earth and Planetary Science Letters* 179(3-4), 437-51.

763 KALASWAD, S., RODEN, M. K., MILLER, D. S. & MORISAWA, M. 1993. Evolution of the
764 continental margin of western India: New evidence from apatite fission-track dating.
765 *Journal of Geology* 101, 667-73.
766 KIRSTEIN, L. A., FOEKEN, J. P. T., VAN DER BEEK, P., STUART, F. M. & PHILLIPS, R. J. 2009.
767 Cenozoic unroofing history of the Ladakh Batholith, western Himalaya constrained by
768 thermochronology and numerical modeling. *Journal of the Geological Society* 166, 667–
769 78, doi:10.1144/0016-7649.2008-107.
770 KIRSTEIN, L. A., SINCLAIR, H. D., STUART, F. M. & DOBSON, K. 2006. Rapid early Miocene
771 exhumation of the Ladakh batholith, western Himalaya. *Geology* 34(12), 1049–52, doi:
772 10.1130/G22857A.
773 KROL, M. A., ZEITLER, P. K. & COPELAND, P. 1996. Episodic unroofing of the Kohistan
774 Batholith, Pakistan: Implications from K-feldspar thermochronology. *Journal of*
775 *Geophysical Research-Solid Earth* 101(B12), 28149-64.
776 KROON, D., STEENS, T. & TROELSTRA, S. R. 1991. Onset of Monsoonal related upwelling in the
777 western Arabian Sea as revealed by planktonic foraminifers. In *Proceedings of the Ocean*
778 *Drilling Program, Scientific Results* eds W. Prell and N. Niitsuma). pp. 257–63. College
779 Station, TX: Ocean Drilling Program. 117, 257–63.
780 KUMAR, A., LAL, N., JAIN, A. K. & SORKHABI, R. B. 1995. Late Cenozoic-Quaternary thermo-
781 tectonic history of Higher Himalayan Crystalline (HHC) in Kishtwar-Padar-Zanskar
782 region, NW Himalaya; evidence from fission track ages. *Journal of the Geological Society*
783 *of India* 45(4), 375-91.
784 LASLETT, G. M., GREEN, P. F., DUDDY, I. R. & GLEADOW, A. J. W. 1987. Thermal annealing of
785 fission track grains in apatite. *Chemical Geology* 65, 1–13.
786 LAVÉ, J. & AVOUAC, J. P. 2001. Fluvial incision and tectonic uplift across the Himalaya of
787 central Nepal. *Journal of Geophysical Research* 106, 26,561–26,92, doi:
788 10.1029/2001JB000359.
789 LEE, J. I., CLIFT, P. D., LAYNE, G., BLUM, J. & KHAN, A. A. 2003. Sediment flux in the modern
790 Indus River traced by the trace element composition of detrital amphibole grains.
791 *Sedimentary Geology* 160, 243–57, DOI:10.1016/S0037-0738(02)00378-0.
792 LI, G., TIAN, Y., KOHN, B. P., SANDIFORD, M., XU, Z. & CAI, Z. 2015. Cenozoic low temperature
793 cooling history of the Northern Tethyan Himalaya in Zedang, SE Tibet and its
794 implications. *Tectonophysics* 643, 80-93, doi:10.1016/j.tecto.2014.12.014.
795 LI, Y., CLIFT, P. D. & O'SULLIVAN, P. 2019. Millennial and Centennial Variations in Zircon U-Pb
796 and Apatite Fission Track Ages in the Quaternary Indus Submarine Canyon. *Basin*
797 *Research* 31, 155–70, doi:10.1111/bre.12313.
798 MEIGS, A. J., BURBANK, D. W. & BECK, R. A. 1995. Middle-late Miocene (>10 Ma) formation of
799 the Main Boundary thrust in the western Himalaya. *Geology* 23(5), 423-26.
800 MÉTIVIER, F., GAUDEMER, Y., TAPPONNIER, P. & KLEIN, M. 1999. Mass accumulation rates in
801 Asia during the Cenozoic. *Geophysical Journal International* 137(2), 280-318.
802 MILES, P. R. & ROEST, W. R. 1993. Earliest seafoor spreading magnetic anomalies in the north
803 Arabian Sea and the ocean-continent transition. *Geophysical Journal International* 115,
804 1025-31.
805 MISHRA, R., PANDEY, D. K., RAMESH, P. & CLIFT, P. D. 2016. Identification of new deep sea
806 sinuous channels in the eastern Arabian Sea. *SpringerPlus* 5, 844, doi:10.1186/s40064-
807 016-2497-6.

MUGNIER, J.-L., HUYGHE, P., CHALARON, E. & MASCLE, G. 1994. Recent movements along the Main Boundary Thrust of the Himalayas: Normal faulting in an over-critical thrust wedge? *Tectonophysics* 238(1–4), 199–215.

NAJMAN, Y. 2006. The detrital record of orogenesis: A review of approaches and techniques used in the Himalayan sedimentary basins. *Earth-Science Reviews* 74(1-2), 1-72.

NAJMAN, Y., APPEL, E., BOUDAGHER-FADEL, M., BOWN, P., CARTER, A., GARZANTI, E., GODIN, L., HAN, J., LIEBKE, U., OLIVER, G., PARRISH, R. & VEZZOLI, G. 2010. Timing of India-Asia collision: Geological, biostratigraphic, and palaeomagnetic constraints. *Journal of Geophysical Research* 115(B12416), doi:10.1029/2010JB007673.

NAJMAN, Y., BICKLE, M., GARZANTI, E., PRINGLE, M., BARFOD, D., BROZOVIC, N., BURBANK, D. & ANDO, S. 2009. Reconstructing the exhumation history of the Lesser Himalaya, NW India, from a multitechnique provenance study of the foreland basin Siwalik Group. *Tectonics* 28(TC5018), doi:10.1029/2009TC002506.

PANDEY, D. K., CLIFT, P. D., KULHANEK, D. K., ANDÒ, S., BENDLE, J. A. P., BRATENKOV, S., GRIFFITH, E. M., GURUMURTHY, G. P., HAHN, A., IWAI, M., KHIM, B.-K., KUMAR, A., KUMAR, A. G., LIDDY, H. M., LU, H., LYLE, M. W., MISHRA, R., RADHAKRISHNA, T., ROUTLEDGE, C. M., SARASWAT, R., SAXENA, R., SCARDIA, G., SHARMA, G. K., SINGH, A. D., STEINKE, S., SUZUKI, K., TAUXE, L., TIWARI, M., XU, Z. & YU, Z. 2016a. Site U1456. In *Arabian Sea Monsoon. Proceedings of the International Ocean Discovery Program* eds D. K. Pandey, P. D. Clift and D. K. Kulhanek). College Station, TX: International Ocean Discovery Program. 355, doi:10.14379/iodp.proc.355.103.2016.

PANDEY, D. K., CLIFT, P. D., KULHANEK, D. K. & EXPEDITION 355 SCIENTISTS 2016b. Arabian Sea Monsoon: Expedition Summary. *Proceedings of the International Ocean Discovery Program* 355, 1-32, doi:10.14379/iodp.proc.355.101.2016.

PANDEY, O. P., AGRAWAL, P. K. & NEGI, J. G. 1995. Lithospheric structure beneath Laxmi Ridge and late Cretaceous geodynamic events. *Geo-Marine Letters* 15, 85-91.

POUPEAU, G., PECHER, A., BENHARBIT, M. & NOYAN, O. F. 1991. Ages traces de fission sur apatites et taux de denudation plio-quaternaires au Karakorum central. *Comptes Rendus de l'Academie des Sciences, Serie II Sciences de la Terre et des Planetes* 313(8), 917-22.

PRELL, W. L., MURRAY, D. W., CLEMENS, S. C. & ANDERSON, D. M. 1992. Evolution and variability of the Indian Ocean Summer Monsoon: evidence from the western Arabian Sea drilling program. In *Synthesis of results from scientific drilling in the Indian Ocean* eds R. A. Duncan, D. K. Rea, R. B. Kidd, U. von Rad and J. K. Weissel). pp. 447–69. Washington, DC: American Geophysical Union. Geophysical Monograph, 70, 447–69.

QUADE, J., CERLING, T. E. & BOWMAN, J. R. 1989. Development of Asian monsoon revealed by marked ecological shift during the latest Miocene in northern Pakistan. *Nature* 342(6246), 163-66.

SADLER, P. M. & JEROLMACK, D. J. 2014. Scaling laws for aggradation, denudation and progradation rates: the case for time-scale invariance at sediment sources and sinks. In *Strata and Time: Probing the Gaps in Our Understanding* eds D. G. Smith, R. J. Bailey, P. M. Burgess and A. J. Fraser). London: Geological Society. Special Publications, 404, doi:10.1144/SP404.7.

SEARLE, M. P. 1996. Cooling history, erosion, exhumation and kinematics of the Himalaya-Karakoram-Tibet orogenic belt. In *The Tectonic Evolution of Asia* eds A. Yin and T. M. Harrison). pp. 110-37. Cambridge: Cambridge University Press. 110-37.

SINGH, S., PARKASH, B., AWASTHI, A. K. & KUMAR, S. 2011. Late Miocene record of palaeovegetation from Siwalik palaeosols of the Ramnagar sub-basin, India. *Current Science* 100(2), 213-22.

STEWART, R. J., HALLET, B., ZEITLER, P. K., MALLOY, M. A., ALLEN, C. M. & TRIPPETT, D. 2008. Brahmaputra sediment flux dominated by highly localized rapid erosion from the easternmost Himalaya. *Geology* 36(9), 711–14, doi: 10.1130/G24890A.1.

SZULC, A. G., NAJMAN, Y., SINCLAIR, H. D., PRINGLE, M., BICKLE, M., CHAPMAN, H., GARZANTI, E., ANDO, S., HUYGHE, P., MUGNIER, J.-L., OJHA, T. & DECELLES, P. G. 2006. Tectonic evolution of the Himalaya constrained by detrital 40Ar/39Ar, Sm/Nd and petrographic data from the Siwalik foreland basin succession, SW Nepal. *Basin Research* 18(4), 375-91.

THIEDE, R. C., BOOKHAGEN, B., ARROWSMITH, J. R., SOBEL, E. R. & STRECKER, M. R. 2004. Climatic control on rapid exhumation along the Southern Himalayan Front. *Earth and Planetary Science Letters* 222(3-4), 791-806.

VAN DER BEEK, P., ROBERT, X., MUGNIER, J.-L., BERNET, M., HUYGHE, P. & LABRIN, E. 2006. Late Miocene-Recent exhumation of the central Himalaya and recycling in the foreland basin assessed by apatite fission-track thermochronology of Siwalik sediments, Nepal. *Basin Research* 18(4), 413-34, doi:10.1111/j.1365-2117.2006.00305.x.

VAN DER BEEK, P., VAN MELLE, J., GUILLOT, S., PÊCHER, A., REINERS, P. W., NICOLESCU, S. & LATIF, M. 2009. Eocene Tibetan plateau remnants preserved in the northwest Himalaya. *Nature Geoscience* 2, 364–68, doi:10.1038/NGEO503.

VANNAY, J.-C., GRASEMANN, B., RAHN, M., FRANK, W., CARTER, A., BAUDRAZ, V. & COSCA, M. 2004. Miocene to Holocene exhumation of metamorphic crustal wedges in the NW Himalaya; evidence for tectonic extrusion coupled to fluvial erosion. *Tectonics* 23(TC1014), doi:10.1029/2002TC001429.

VERMEESCH, P. 2012. On the visualisation of detrital age distributions. *Chemical Geology* 312–313, 190–94, doi:10.1016/j.chemgeo.2012.04.021.

VÖGELI, N., NAJMAN, Y., BEEK, P. V. D., HUYGHE, P., WYNN, P. M., GOVIN, G., VEEN, I. V. D. & SACHSE, D. 2017. Lateral variations in vegetation in the Himalaya since the Miocene and implications for climate evolution. *Earth and Planetary Science Letters* 471, 1–9, doi:10.1016/j.epsl.2017.04.037.

WALLIS, D., CARTER, A., PHILLIPS, R. J., PARSONS, A. J. & SEARLE, M. P. 2016. Spatial variation in exhumation rates across Ladakh and the Karakoram: New apatite fission track data from the Eastern Karakoram, NW India. *Tectonics* 35, 704–21, doi:10.1002/2015TC003943.

WARNER, L. F. 1993. Variable denudation of the Nanga Parbat-Haramosh Massif: A fission track study of the Tato Valley, Pakistan. p. 34. Bethlehem, PA: Lehigh University.

WASSON, R. J. 2003. A sediment budget for the Ganga–Brahmaputra catchment. *Current Science* 84(3), 1041-47.

WEBB, A. A. G. 2013. Preliminary palinspastic reconstruction of Cenozoic deformation across the Himachal Himalaya (northwestern India). *Geosphere* 9, 572-87.

WHITE, N. M., PRINGLE, M., GARZANTI, E., BICKLE, M., NAJMAN, Y., CHAPMAN, H. & FRIEND, P. 2002. Constraints on the exhumation and erosion of the High Himalayan Slab, NW India, from foreland basin deposits. *Earth and Planetary Science Letters* 195, 29-44.

WILLENBRING, J. K. & VON BLANCKENBURG, F. 2010. Long-term stability of global erosion rates and weathering during late-Cenozoic cooling. *Nature* 465, 211-14, doi:10.1038/nature09044.

ZEILINGER, G., BURG, J. P., SCHALTEGGER, U. & SEWARD, D. 2001. New U/Pb and fission track ages and their implication for the tectonic history of the lower Kohistan Arc Complex, northern Pakistan. *Journal of Asian Earth Sciences* 19(3S), 79-81.

ZEITLER, P. K. 1985. Cooling History of the NW Himalaya, Pakistan. *Tectonics* 4(1), 127-51.

ZEITLER, P. K., CHAMBERLAIN, C. P. & SMITH, H. A. 1993. Synchronous Anatexis, Metamorphism, and Rapid Denudation at Nanga-Parbat (Pakistan Himalaya). *Geology* 21(4), 347-50.

ZEITLER, P. K., SUTTER, J. F., WILLIAMS, I. S., ZARTMAN, R. E. & TAHIRKHELI, R. A. K. 1989. Geochronology and temperature history of the Nanga Parbat-Haramosh Massif, Pakistan. In *Tectonics of the western Himalayas* eds L. L. Malinconico and R. J. Lillie). pp. 1–22. Boulder, CO: Geological Society of America. Special Paper, 232, 1–22.

ZHANG, P., MOLNAR, P. & DOWNS, W. R. 2001. Increased sedimentation rates and grain sizes 2–4 Myr ago due to the influence of climate change on erosion rates. *Nature* 410, 891–97.

ZHUANG, G., NAJMAN, Y., TIAN, Y., CARTER, A., GEMIGNANI, L., WIJBRANS, J., JAN, M. Q. & KHAN, M. A. 2018. Insights into the evolution of the Hindu Kush-Kohistan-Karakoram from modern river sand detrital geo- and thermochronological studies. *Journal of the Geological Society*, doi:10.1144/jgs2018-007.

Lab No.	IODP Sample Name	Depositional Age (Ma)	Depth (mbsf)	AFT Minimum Age (Ma)	2σ (Ma)	Number of grains	Zircon U-Pb ages
134-1	U1456A-11H-6 60-69 cm	0.93	97.60	20.70	3.80	24	Yes
134-2	U1456A-26F-3 50-58 cm	1.32	185.91	3.60	0.85	62	
134-3	U1456A-51F-3 100-110 cm	1.56	302.09	3.90	1.40	44	Yes
134-4	U1456A-61F-3 40-50 cm	1.92	345.32	6.50	1.10	45	Yes
177-1	U1456A-70F-2 10-16 cm	3.02	386.73	5.70	1.50	75	Yes
177-12	U1457C-31R-1 94-100 cm	3.17	474.25	5.10	1.80	52	
177-13	U1457C-33R-3 10-17 cm	3.43	499.10	6.40	1.20	49	Yes
177-2	U1456C-45X-3 45-51 cm	3.57	459.09	8.48	0.75	65	
134-6	U1456D-5R-1 12-20 cm	5.72	487.98	9.30	2.20	50	Yes
177-14	U1457C-41R-2 20-26 cm	5.78	572.16	5.91	0.83	46	
177-15	U1457C-42R-1 80-88 cm	5.82	580.40	6.40	1.10	55	
177-16	U1457C-43R-1 55-63 cm	5.87	590.53	9.00	1.20	57	Yes
177-3	U1456D-12R-1 30-36 cm	7.00	556.45	6.60	1.50	52	
177-4	U1456D-13R-1 30-38 cm	7.07	566.35	13.20	7.30	30	Yes
177-5	U1456D-15R-1 55-61 cm	7.28	586.00	15.80	1.90	50	
177-6	U1456D-19R-2 20-26 cm	7.66	625.73	11.90	1.80	40	
177-17	U1457C-51R-4 80-88 cm	7.78	675.16	12.00	3.20	51	
134-7	U1456D-22R-1 73-83 cm	7.84	653.50	15.48	0.97	69	Yes
134-10	U1457C-61R-1 8-18 cm	7.99	769.36	14.00	3.10	42	
177-8	U1456D-26R-2 37-43 cm	8.09	693.78	14.90	1.60	55	
177-9	U1456D-27R-2 100-106 cm	8.15	704.43	16.97	0.98	69	
177-10	U1456D-28R-1 40-46 cm	8.20	711.98	14.20	1.80	72	
134-8	U1456D-29R-2 24-34 cm	8.27	722.60	11.80	5.30	64	Yes
134-9	U1456E-19R-3 10-20 cm	15.58	1102.95	20.20	1.40	75	Yes

Table 1

	Lab No	Sample	Dep. Age	No. of	Dosimeter								Central Age	Minimum Age	P2 Age
			(Ma)	grains	ρd	Nd	ρs	Ns	ρi	Ni	Pχ^2	RE%	(Ma)	(Ma)	(Ma)
A	134-1	U1456A-11H-6 60-69 cm	0.93	24	1.583	4388	0.798	218	3.858	1440	0	111	61.2±14.9	20.7±3.8	223±28
B	134-2	U1456A-26F-3 50-58 cm	1.32	62	1.583	4388	0.108	308	3.555	11836	0	79	7.3±0.9	3.6±0.9	13.4±1.3
C	134-3	U1456A-51F-3 100-110 cm	1.56	44	1.583	4388	0.191	298	6.856	12192	0	70	6.8±0.9	3.9±1.4	7.2±0.9
D	134-4	U1456A-61F-3 40-50 cm	1.92	45	1.583	4388	0.178	349	5.498	11649	0	35.2	8.1±35.2	6.5±1.1	
E	177-1	U1456A-70F-2 10-16 cm	3.02	75	1.215	3367	0.206	446	4.539	11389	0	54.2	8.2±0.7	5.7±1.5	15.5±2.3
F	177-12	U1457C-31R-1 94-100 cm	3.17	75	1.215	3367	0.171	326	4.710	10359	0	51.5	6.8±0.6	5.1±1.8	12.7±2.1
G	177-13	U1457C-33R-3 10-17 cm	3.43	49	1.215	3367	0.211	313	4.528	8601	0	50.8	7.7±0.8	6.4±1.2	
H	177-2	U1456C-45X-3 45-51 cm	3.57	65	1.215	3367	0.349	474	4.737	9089	0	160	12.9±2.7	8.5±0.8	
I	134-6	U1456D-5R-1 12-20 cm	5.72	50	1.583	4388	0.272	314	6.211	7830	0	42.4	11.2±1.0	9.3±2.2	
J	177-14	U1457C-41R-2 20-26 cm	5.78	46	1.215	3367	0.186	236	3.801	6317	0	180	11.4±3.1	5.9±0.8	
K	177-15	U1457C-42R-1 80-88 cm	5.82	55	1.215	3367	0.179	361	4.073	9719	0	160	7.8±0.8	6.4±1.1	15.9±2.6
L	177-16	U1457C-43R-1 55-63 cm	5.87	80	1.215	3367	0.389	528	5.048	8747	0	12.4	13.7±1.6	9.0±1.2	29.4±1.2
M	177-3	U1456D-12R-1 30-36 cm	7.00	52	1.215	3367	0.241	347	4.004	6997	0	53.8	10.7±1.0	6.6±1.7	17.7±1.7
N	177-4	U1456D-13R-1 30-38 cm	7.07	30	1.215	3367	0.297	124	5.000	2061	2.1	44.7	11.4±1.5	11.4±1.5	
O	177-5	U1456D-15R-1 55-61 cm	7.28	50	1.215	3367	0.362	372	3.718	4683	0	39.2	16.5±1.3	15.8±1.9	
P	177-6	U1456D-19R-2 20-26 cm	7.66	40	1.215	3367	0.546	457	4.714	4931	0	73.4	19.9±2.6	11.9±1.8	28.0±4.7
Q	177-17	U1457C-51R-4 80-88 cm	7.78	51	1.215	3367	0.326	430	4.140	5605	0	40	14.7±1.2	12.0±3.2	19.9±1.6
R	134-7	U1456D-22R-1 73-83 cm	7.84	80	1.583	4388	0.424	799	6.226	12387	0	44.6	18.6±1.2	15.5±0.9	
S	134-10	U1457C-61R-1 8-18 cm	7.99	42	1.583	4388	0.353	468	5.490	7570	0	14.3	16.1±1.0	14.0±3.1	
T	177-8	U1456D-26R-2 37-43 cm	8.09	55	1.215	3367	0.337	403	3.651	5056	0	48.9	18.4±1.7	14.9±1.6	
U	177-9	U1456D-27R-2 100-106 cm	8.15	92	1.215	3367	0309	605	3.710	7958	0	41.8	16.0±1.0	16.9±0.9	
V	177-10	U1456D-28R-1 40-46 cm	8.20	72	1.215	3367	0.499	639	5.203	7453	0	73.3	18.4±1.8	14.2±1.8	21.1±1.9
W	134-8	U1456D-29R-2 24-34 cm	8.27	72	1.583	4388	0.424	639	5.508	9347	0	48.6	19.3±1.4	11.8±5.3	38.8±3.8
X	134-9	U1456E-19R-3 10-20 cm	15.58	75	1.583	4388	0.462	873	4.957	9653	0	55.9	25.9±2.0	20.2±1.4	

Table 2. Summary of apatite fission track analytical data. Track densities are ($x10^6$ tr cm^{-2}) numbers of tracks counted (N) shown in brackets. Analyses by external detector method using 0.5 for the 4p/2p geometry correction factor. Ages calculated using dosimeter glass CN-5; (apatite) ζ_{CN5} =338±5; calibrated by multiple analyses of IUGS apatite and zircon age standards (Hurford, 1990). Pχ^2 is probability for obtaining c^2value for v degrees of freedom, where v = no. crystals – 1. Central age is a modal age, weighted for different precisions of individual crystals (see Galbraith (1990)). Minimum age model after Galbraith (2005). P2 used peak fitting algorithm of Galbraith and Green, (1990) where there are >10 grains.

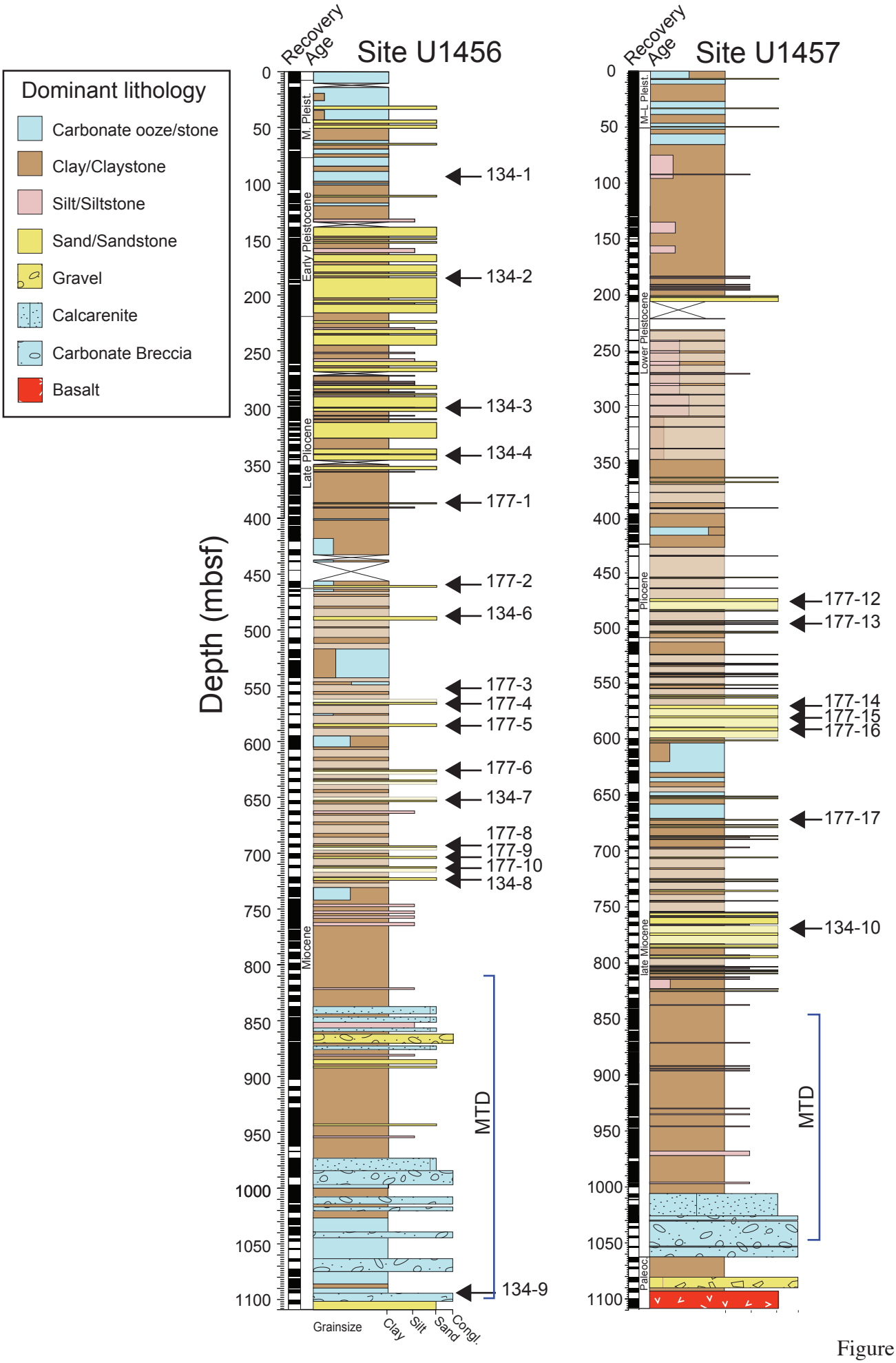

Figure 2
Zhou et al.

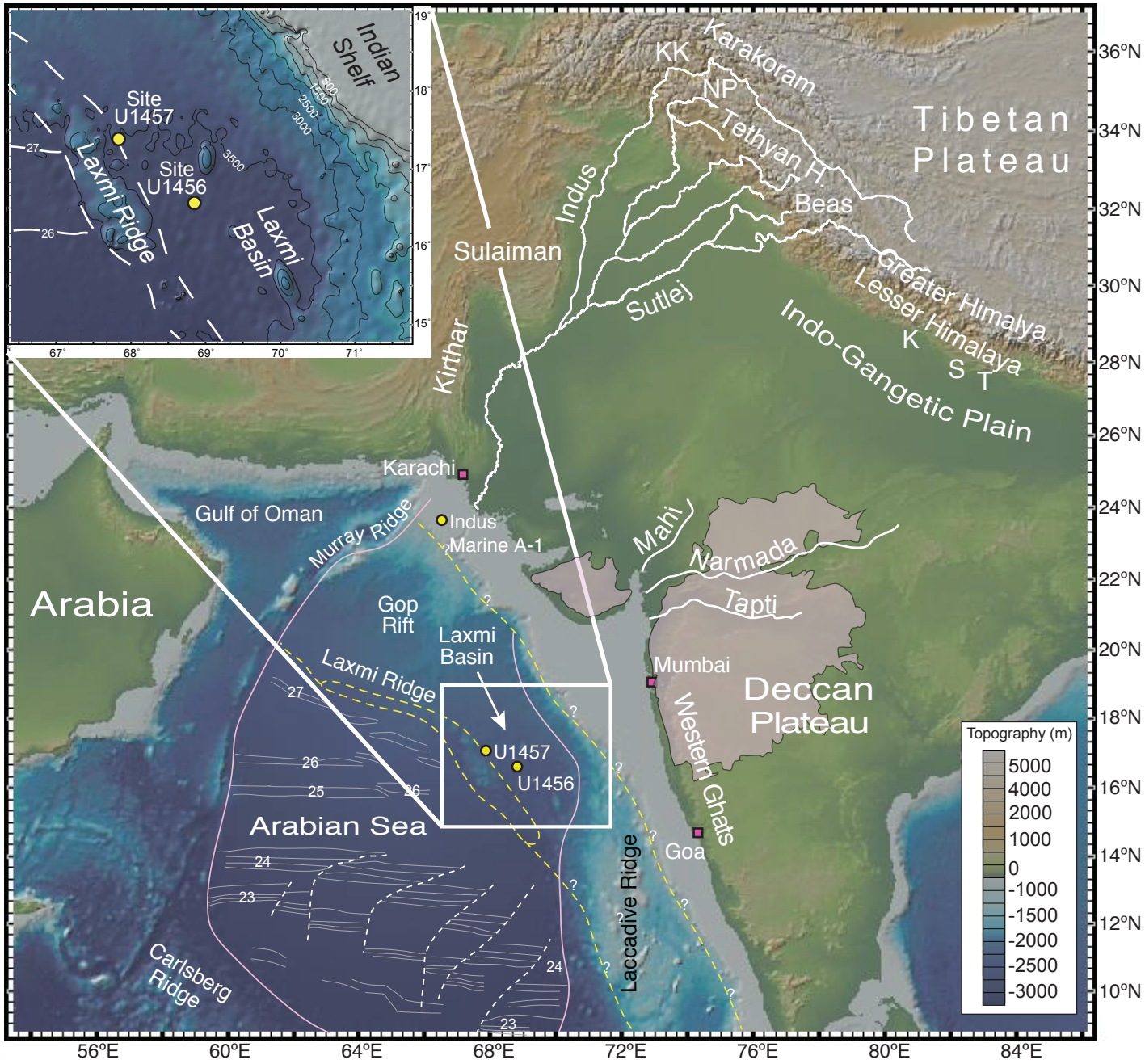

Figure 1
Zhou et al.

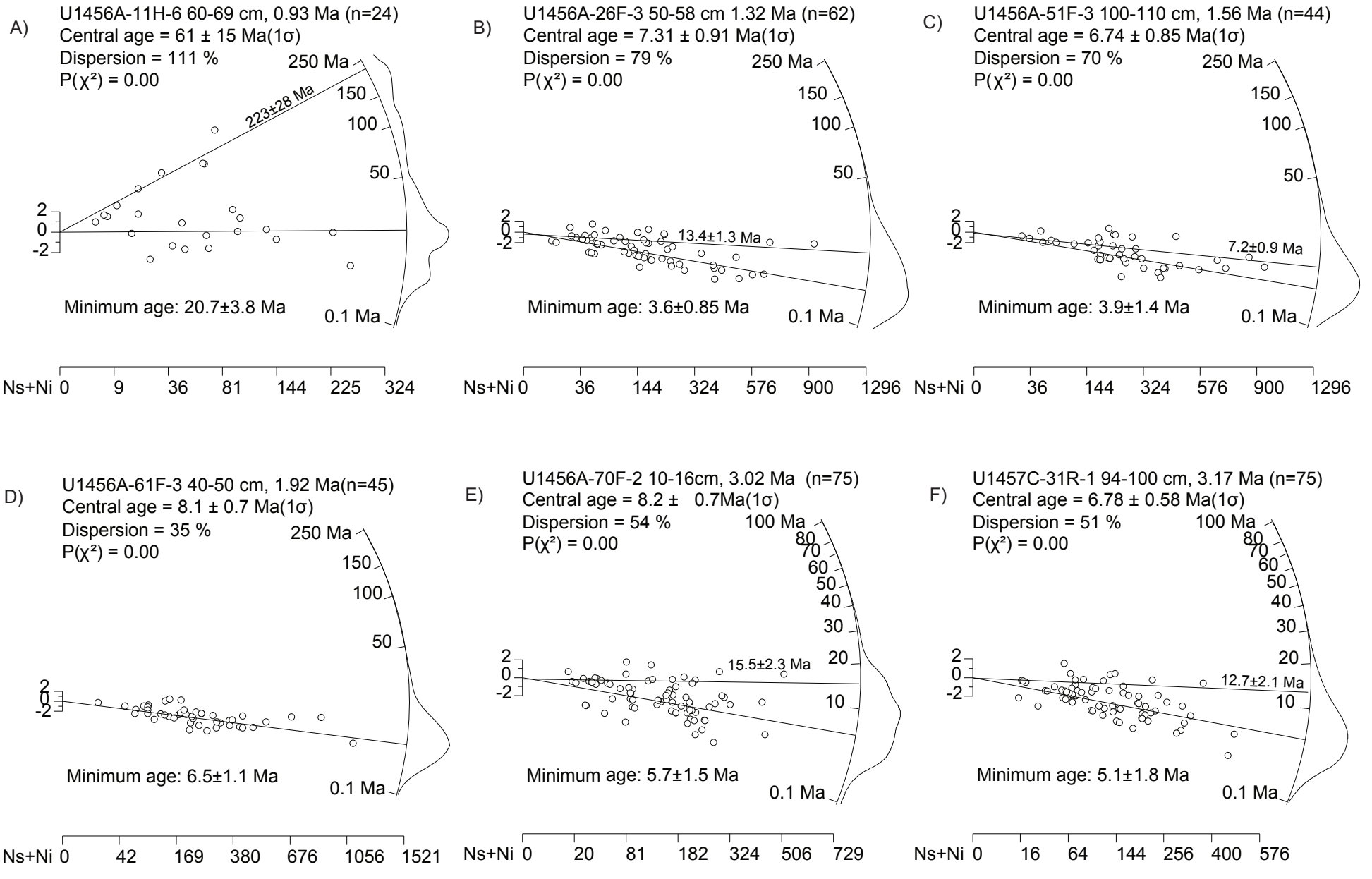

Figure 3
Zhou et al.

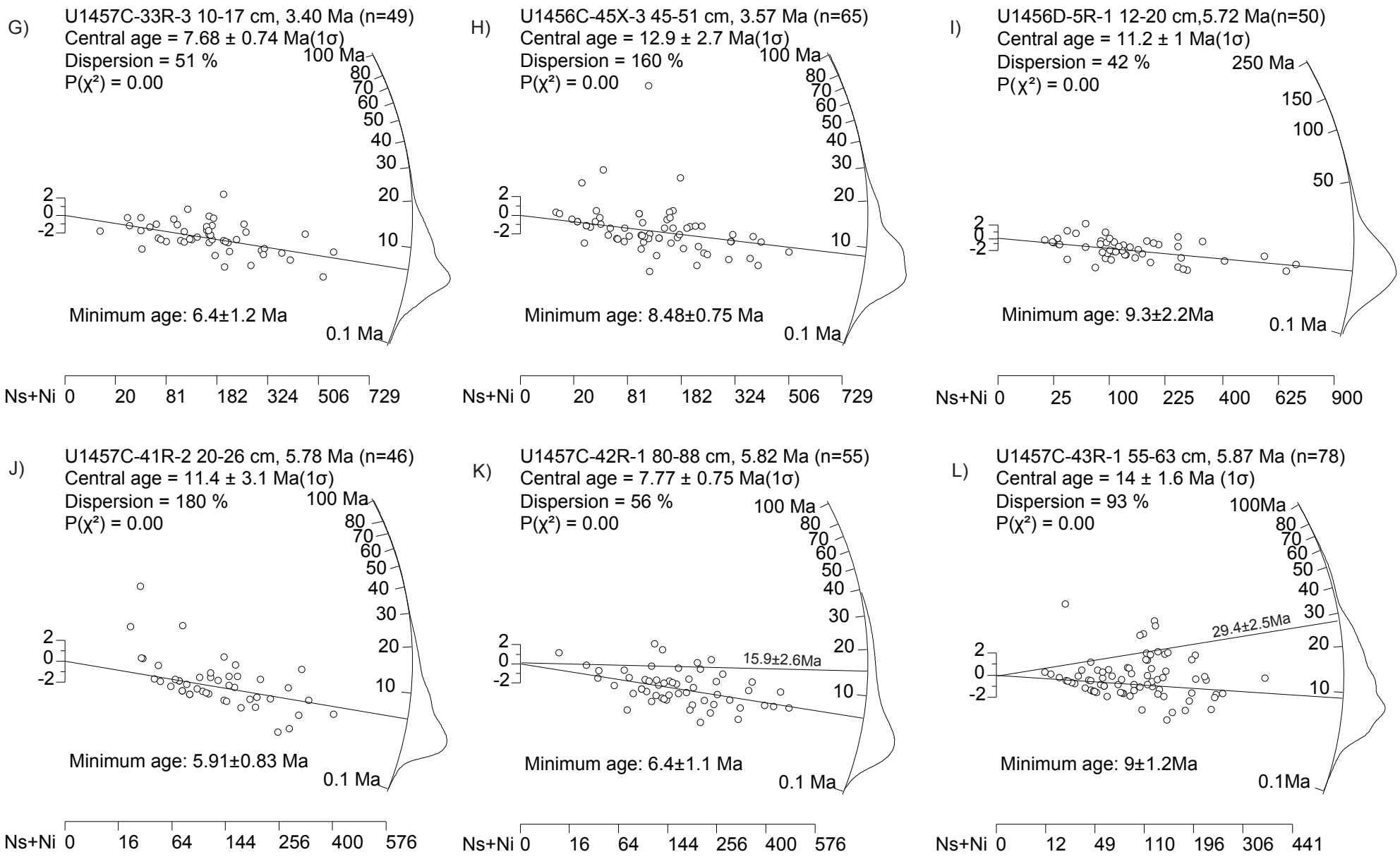

Figure 3
Zhou et al.

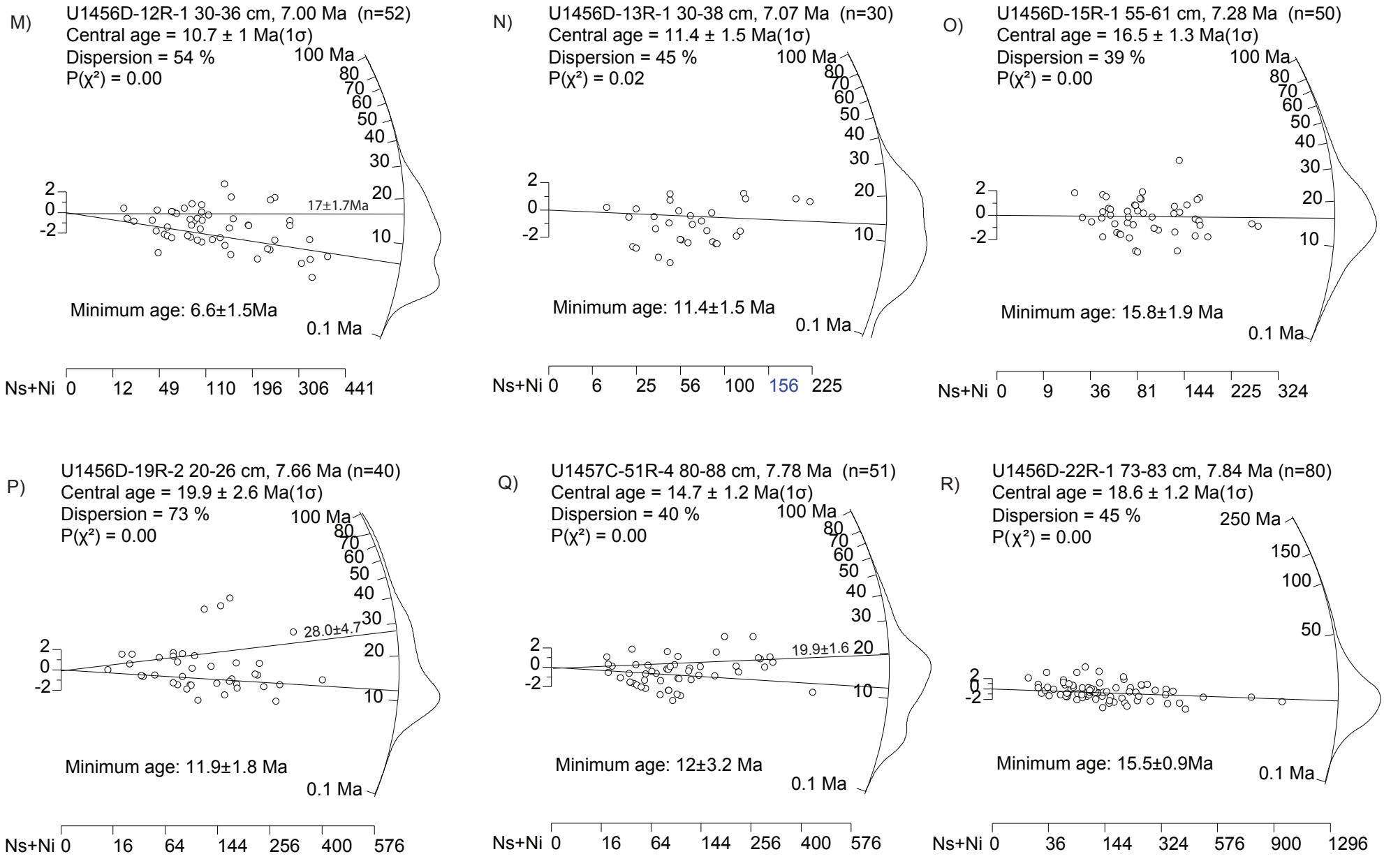

Figure 3
Zhou et al.

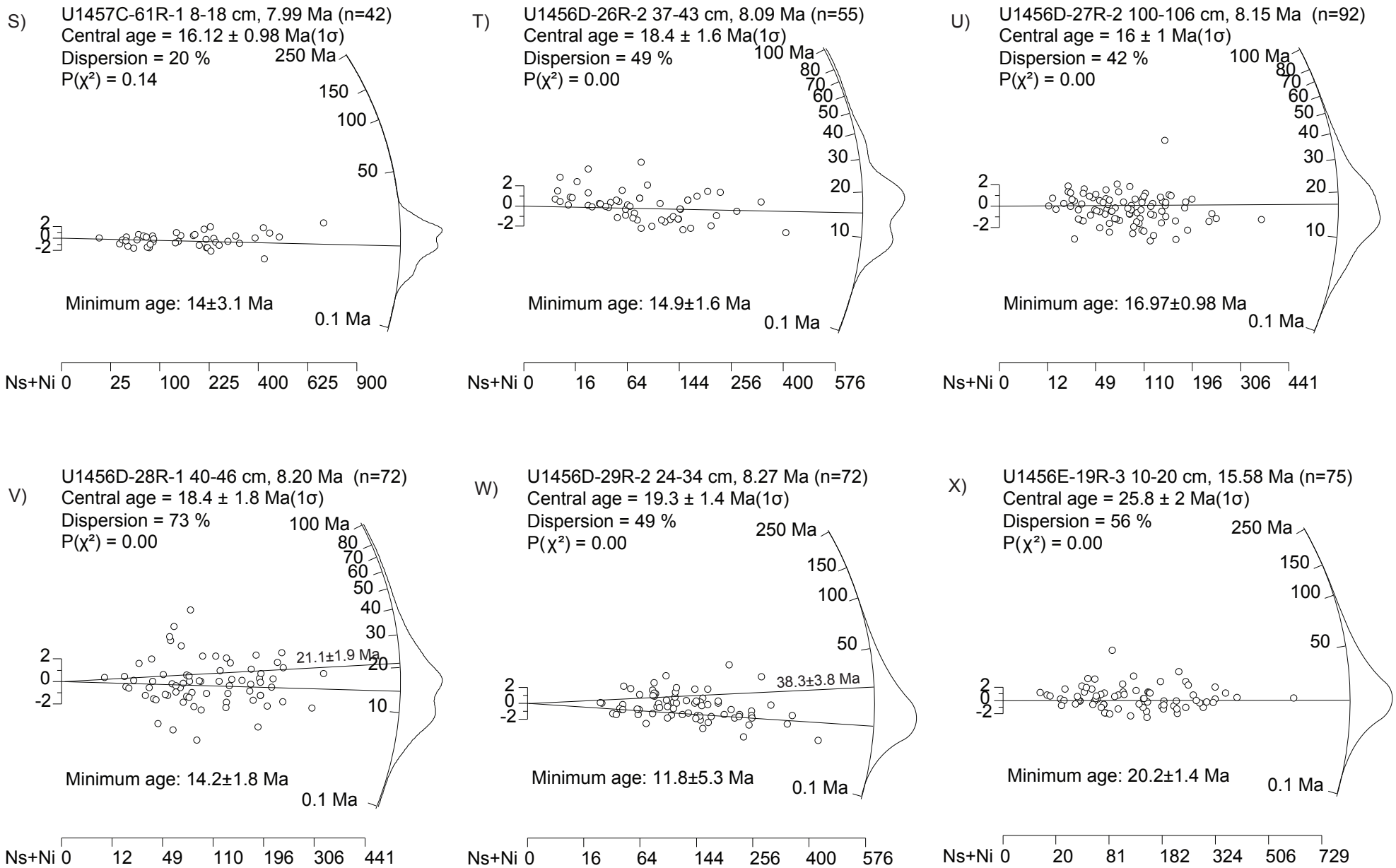

Figure 3
Zhou et al.

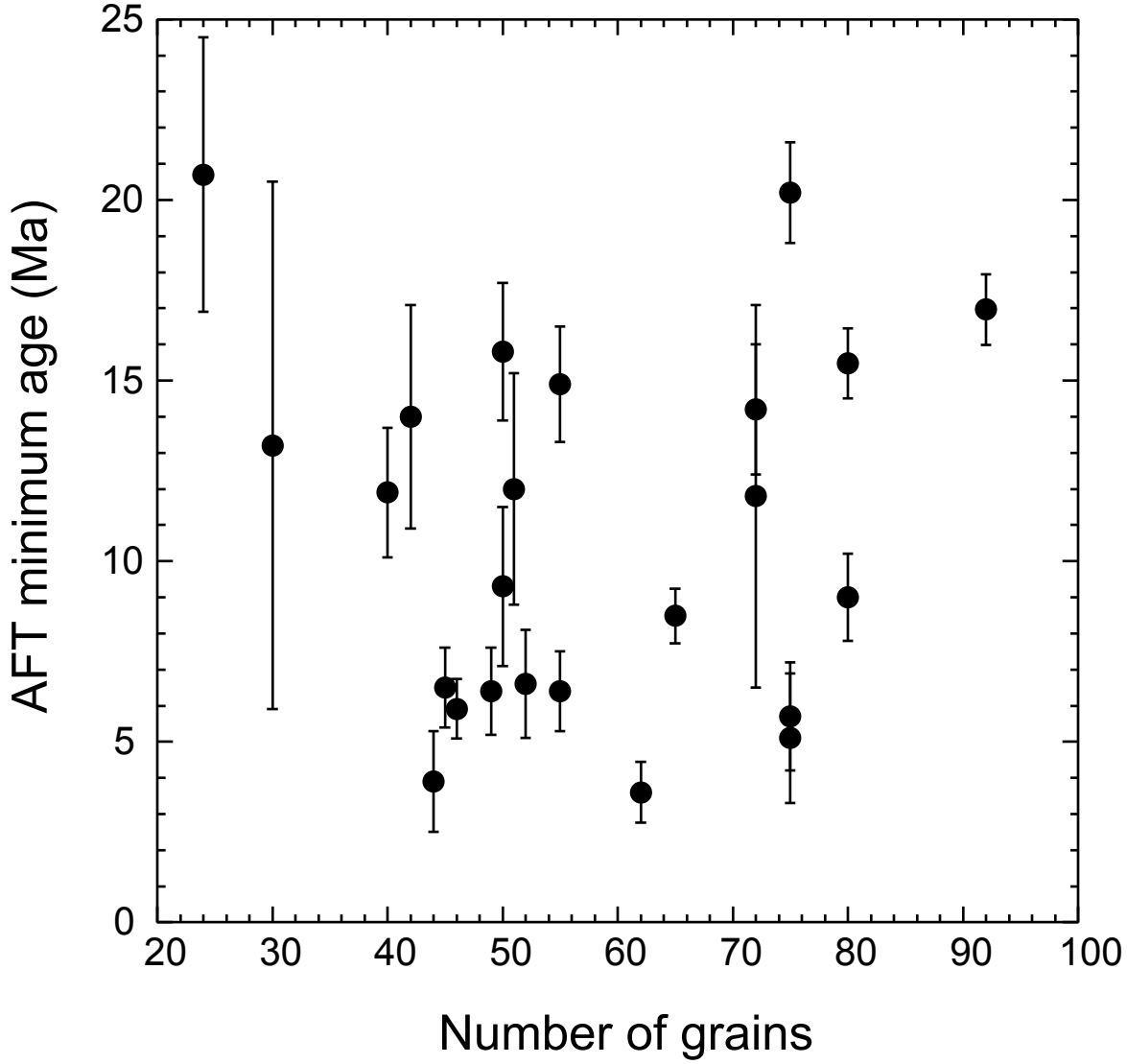

Figure 4
Zhou et al.

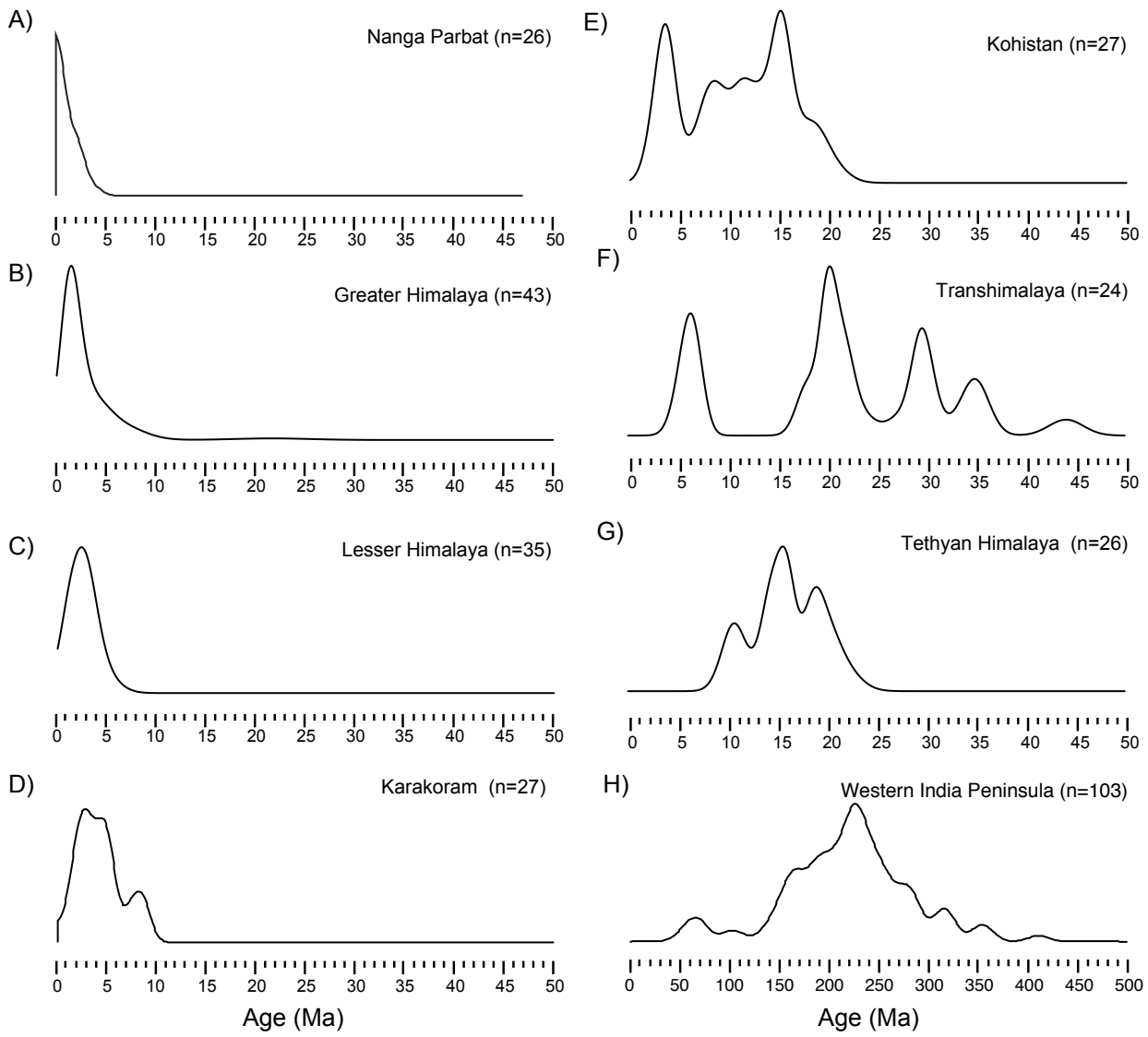

Figure 5
Zhou et al.

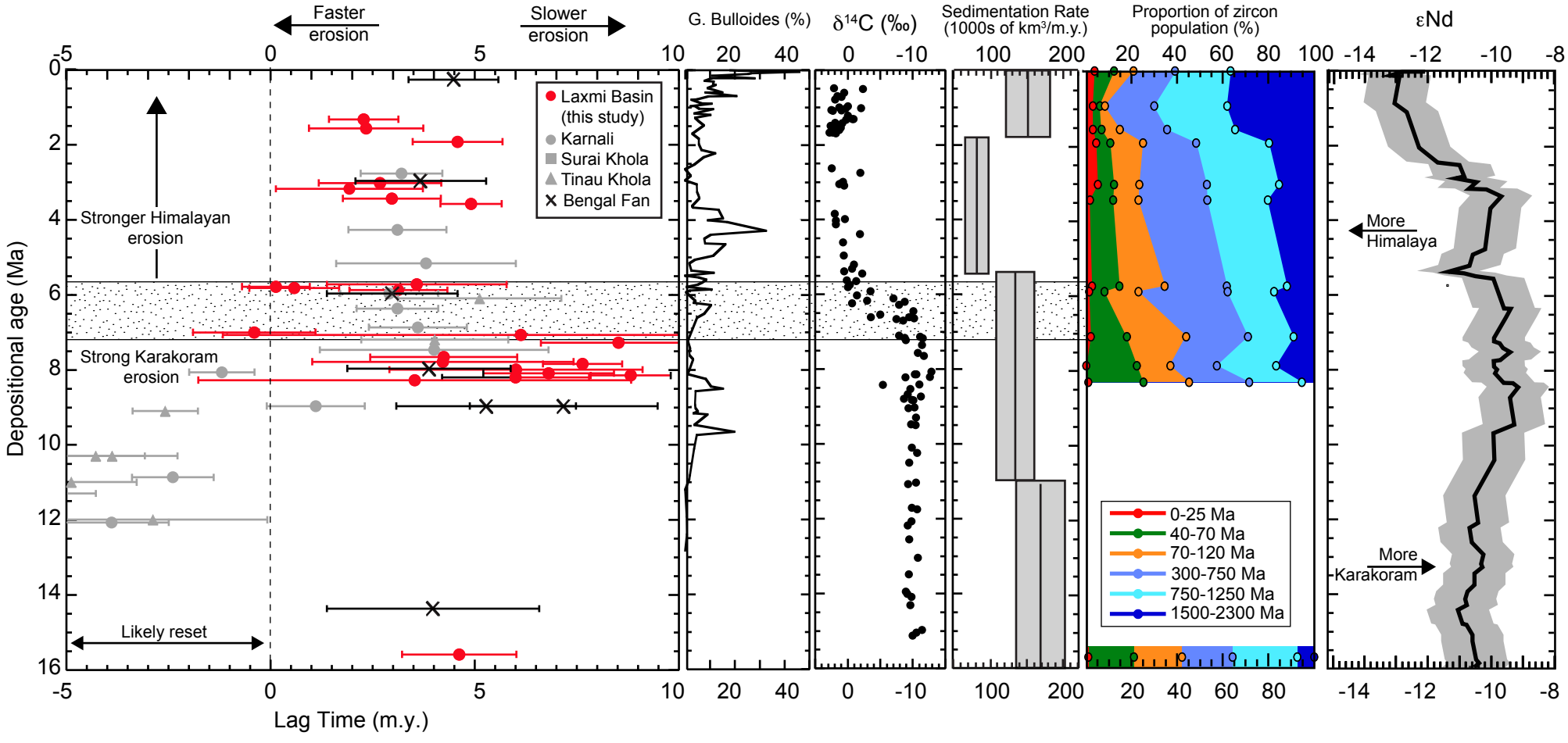

Figure 6
Zhou et al.